Non-destructive evaluation of plate-like concrete structures: elastic properties and thickness

OSKAR BAGGENS
DIVISION OF ENGINEERING GEOLOGY | LUND UNIVERSITY

Licentiate thesis

Non-destructive evaluation of plate-like concrete structures: elastic properties and thickness

Oskar Baggens,
Division of Engineering Geology,
Lund University, Sweden

oskar.baggens@tg.lth.se

ISBN: 978-91-7623-259-0 (print)
ISBN: 978-91-7623-260-6 (web/pdf)
ISRN LUTVDG/(TVTG-1033)/1-93/2015

☼2015-02-26 ◷08:44:31

Abstract

There exists an increased demand for techniques applicable for non-destructive evaluation of concrete structures. The impact-echo method, which is based on the evaluation of the structural response to a transient impact is one available alternative. Typically, impact-echo measurements are used to detect flaws in concrete structures by monitoring the *relative* variation in the resonance frequency of the response. Another possible application of the impact-echo method is material characterization. By combining impact-echo with measurements of surface waves and the theory of Lamb waves, material properties and thickness of plate-like structures can be estimated. This thesis is focused on the study of this approach for non-destructive material characterization.

Results from practical testing using the impact-echo method, as well as the combined impact-echo and surface wave approach, indicate a systematic error which underestimates the thickness. This systematic error is studied in the first appended paper and found to be dependent on the distance to the excitation source, i.e. a so-called near-field effect. A major source of uncertainty contributing to the systematic error is related to the estimation of the longitudinal wave velocity along the plate surface.

With motivation of the results presented in Paper I, an alternative approach for estimation of Poisson's ratio is proposed in the second appended paper. The proposed approach is based on the evaluation of the amplitude ratio of the surface normal and surface in-plane component of the first symmetric zero-group velocity Lamb mode. Thus, this approach is not dependent on an estimation of the longitudinal wave velocity along the surface. Furthermore, the approach provides an estimation of Poisson's ratio which is representative through the entire plate thickness. A practical field case shows an increased accuracy of the estimated nominal plate thickness from this approach compared with the traditional approach based on the longitudinal wave velocity.

Sammanfattning

Det finns ett ökande behov av metoder som kan användas för oförstörande provning av betongkonstruktioner. Ett alternativ är metoden impact-echo som bygger på utvärderingen av responsen hos en konstruktion efter ett transient slag. Vanligtvis används impact-echo för att detektera skador och avvikelser genom att den relativa variationen av resonansfrekvensen hos konstruktionens respons studeras. Ett annat användningsområde för impact-echo är bestämning av materialegenskaper. Genom att kombinera impact-echo med mätningar av ytvågor och teori för Lamb vågor är det möjligt att bestämma materialegenskaper och tjockleken hos plattliknande konstruktioner. Den här licentiatuppsatsen fokuserar på denna typ av metod för oförstörande bestämning av materialegenskaper.

Resultat från mätningar med impact-echo indikerar ett systematiskt fel som underskattar tjockleken. Det gäller även när impact-echo kombineras med mätning av ytvågor. Detta systematiska fel undersöks i den första bifogade artikeln. Felet visar sig bero på avståndet till punktkällan (t.ex. hammarslaget), dvs. en så kallad närfältseffekt. En osäker uppmätt kompressionsvågshastig längs med ytan på plattan är en bidragande orsak till det systematiska felet.

Mot bakgrund av osäkerheten i den uppmätta kompressionsvågshastigheten föreslås i den andra bifogade artikeln en alternativ metod för bedömning av Poisson's tal. Metoden bygger på en utvärdering av kvoten mellan den mot ytan vinkelräta och parallella amplituden hos den första symmetriska Lamb moden med grupphastighet lika med noll. Kompressionsvågshastigheten längs plattans yta behöver därmed inte mätas. Dessutom fås en uppskattning av Poisson's tal som är representativ för hela tjockleken av plattan. I en demonstrerad praktisk mätning fås en förbättrad uppskattning av den nominella tjockleken av plattan med den här metoden, jämfört med den traditionella metoden baserad på en kompressionsvågshastighet.

Preface

The work of this thesis has been carried out at the Division of Engineering Geology, Lund University. The financial support from The Development Fund of the Swedish Construction Industry (SBUF, No. 12534) and The Swedish Radiation Safety Authority (SSM, No. SSM2012-890) is gratefully acknowledged.

I want to thank my main supervisor Nils Rydén for all help, guidance, and excellent support during the entire course of this work. Thank you!

I would also like to thank my assisting supervisors Björn Thunell and Gerhard Barmen. I am also thankful towards Prof. Michael Lowe and Prof. John S. Popovics for valuable help and feedback.

Thanks also to all fellow PhD students for inspiring and interesting discussions, and to my family and friends for support and encouragement.

Last but by no means least, thank you Linda.

Oskar Baggens,
February 2015.

List of appended papers

Paper I

O. Baggens and N. Ryden.
Systematic errors in Impact-Echo thickness estimation due to near field effects. NDT & E International, 69:16-27, Jan. 2015. ISSN 09638695. doi: 10.1016/j.ndteint.2014.09.003.

Paper II

O. Baggens and N. Ryden.
Poisson's ratio from polarization of zero-group velocity Lamb mode. Submitted for publication (Journal of the Acoustical Society of America). 2015.

Related papers

O. Baggens and N. Ryden.
Near field effects and estimation of Poisson's ratio in impact-echo thickness testing, accepted to 41 st Annual Review of Progress in Quantitative Nondestructive Evaluation, Boise, Idaho, 2014. AIP Conference Proceedings.

Contents

Part I

Overview of work

Chapter 1

Introduction

This chapters presents general information about non-destructive techniques, motivation of work, aim and objective, and a summary of the appended papers.

Non-destructive testing (NDT) is a general term which refers to the task of evaluating some sort of property without introducing any permanent damage on the studied object (Shull, 2002). The property of interest can for example be a mechanical material parameter such as acoustic velocity, and the object can for example be a pavement (Ryden et al., 2004). Other examples are identification of defects and flaws in pipelines (Lowe et al., 1998) and composite materials (Castaings et al., 1998). NDT methods are also very common used in medicine, e.g. in the form of ultrasonic and radiography.

Although NDT methods can be very complicated and sophisticated, both from a measurement and evaluation point of view, it is still possible to find simple examples of the basic principles of NDT in our everyday life. A typical and intuitive example is the "tap and listen" principle. Everyone has probably sometime tapped at a object (e.g. a table-top) to find out what type of material it is made of (e.g. stone, massive wood, or plastic). In fact, this type of very simple principle forms the basis for the impact-echo method (Sansalone and Streett, 1997), which can be used to study concrete structures.

Non-destructive techniques are important from a number of different perspectives such as optimization of resources for manufacturing, quality control, condition and damage assessment, etc. Information and results obtained using NDT techniques can be used to plan maintenance, estimate safety status, predict structural lifetime, and also serve as a pay factor. Non-destructive testing techniques can off course not provide

all information about an object, and neither detect all possible defects. One should therefore consider NDT techniques as a complement, not a replacement, to destructive techniques which in some cases may be the only option.

A sound way of thinking about non-destructive methods is to consider all techniques as tools. Typically, a craft man needs several *different* tools in his or her work, since the tools are designed for different purposes. In the same manner, a NDT technician needs different non-destructive techniques in his or her work. In other words it should be noted that there is no such thing as a one method which can measure everything.

1.1 Non-destructive testing of concrete structures

There exist a vast number of different non-destructive techniques which are applicable for testing of concrete structures. Some typical tasks for the techniques are: determining location of reinforcement bars, detecting cracks and voids, measuring thickness, estimating material properties. Another important task is inspection of internal steel parts, such as reinforcement bars or cable ducts, to detect early stages of corrosion. Based on the task in focus, a selection of the appropriate method or combination of methods has to be made. This selection is in some sense a choice of which physical principle that is most relevant for the task.

The following section will present some different non-destructive techniques organized with respect to their used physical principles. The presentation will mainly focus on electromagnetic and acoustic methods, since these are the most widely used techniques for concrete applications, and considered most relevant for the background of this thesis. Note that other non-destructive techniques, e.g. thermography, image analysis etc., also exist. However, it goes outside the scoop of this thesis to cover all possible non-destructive methods available for concrete structures. For a more detailed review of non-destructive techniques available for concrete material and structures, please refer to e.g. Malhotra and Carino (2004).

1.2 Electromagnetic methods

Electromagnetic radiation has a wide range of different applications. Non-destructive testing is one application. Two main families of non-destructive test methods based on electromagnetic waves are radiography and radar. The main difference between these two methods is the frequency or wavelength used. Typically, radiography uses short wavelengths (high frequencies) whereas radar uses long wavelengths (low frequencies).

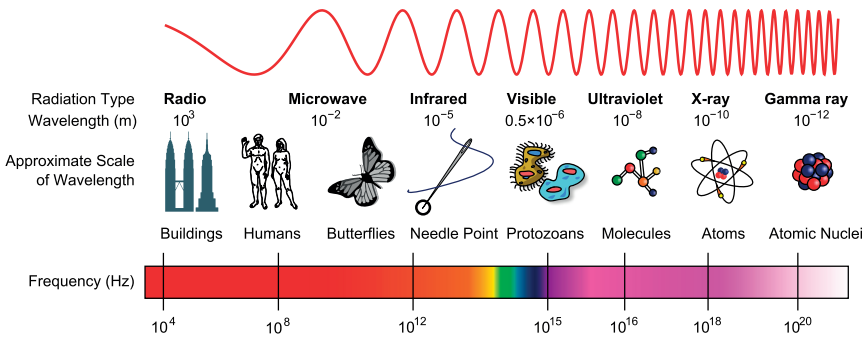

Figure 1.1: Electromagnetic spectrum. Original figure by Inductiveload (licensed under CC BY-SA 3.0)

Figure 1.1 shows an illustration of the electromagnetic spectrum. It can be observed that the visible light only represents a small portion of the spectrum.

1.2.1 Radiography

Radiography is often associated with machines used in hospitals or at the dentist. However, radiography is a general non-destructive technique applicable for many structures. In fact, radiography is the only non-destructive technique which is applicable to any possible material (Shull, 2002). Non-destructive testing of concrete structures using radiography is commonly performed with mobile equipment: in most cases it is not possible to move the structure to stationary equipment. Radiographic techniques are suitable for detailed study of reinforcement bars, cable duct status, void detection, i.e. in cases with many geometric details.

The equipment consists mainly of two parts: radiation source and receiver, see Figure 1.2, which shows a mobile x-ray system. The source sends a radiation beam towards the object of interest. From a simplified point of view, the radiation source basically acts as a very strong light bulb, sending a special kind of light which can pass through the object. The material in the studied volume determines the amount of radiation which passes through the object and reaches the receiver. The receiver measures the amount of absorbed radiation. Figure 1.3 shows an example of result obtained from a x-ray measurement.

Practical use of radiography needs two sided access of the object, and the equipment can be expensive. Furthermore, the actual measurement may require long exposure time (depending on thickness), and the radiation

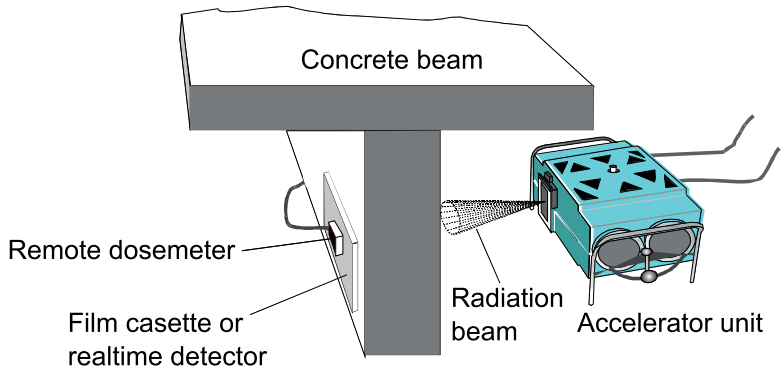

Figure 1.2: Mobile radiographic x-ray system "Betatron". Original figure presented by Shaw et al. (2004).

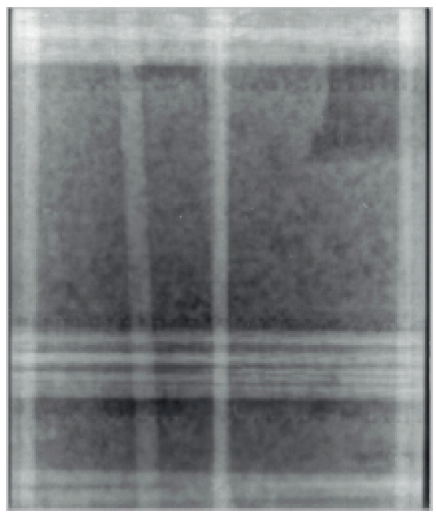

Figure 1.3: Example of image from x-ray measurement of concrete. Reinforcement bars are clearly visible as white/light stripes. Original figure presented by Shaw et al. (2004).

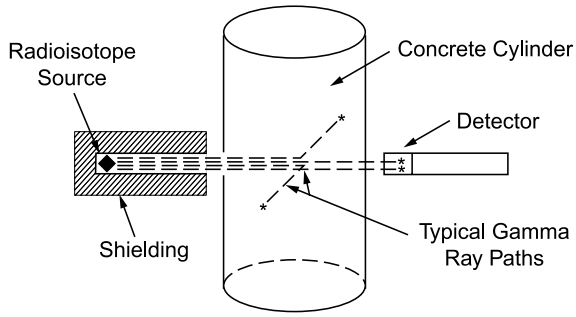

Figure 1.4: Principle sketch of radiography using gamma radiation ("permanent" radiation source). Original figure presented by Malhotra and Carino (2004)

can also be dangerous to humans. For these reasons, radiography is mainly used for point wise inspection of complicated objects when an exact and precise non-destructive evaluation is needed, or under circumstances where other methods may not be applicable.

Two radiation types which can be used in radiographic measurements are gamma radiation and x-rays. Gamma radiation is generated by radioactive isotopes, e.g. Iridium or Cobalt. These isotopes are referred to as "permanent" radiation sources, and are suitable for concrete structure with a thickness up to about 0.3 m (Iridium) and 0.6 m (Cobalt) (Shaw et al., 2004). Figure 1.4 shows an example of measurement using gamma radiation. An alternative to gamma radiation is x-rays which can be used up to thickness of about 1.5 m (Shaw et al., 2004). X-rays are created when electrons which are accelerated to a high energy strike against a metallic object. Figure 1.2 shows an example of measurement set-up using x-rays.

1.2.2 Short-pulse radar

Radar, which is an acronym for **ra**dio **d**etection **a**nd **r**anging, is a technique based on the concept of sending electromagnetic pulses and analyzing received echoes. The echoes are generated when the electromagnetic wave reach an object with different dielectric constant (e.g. a steel part of an aircraft flying in the sky). Radar techniques are nowadays used in a wide range of applications.

The radar technique is also applicable for concrete structures, where frequencies around 500-3000 MHz are commonly used (Shaw et al.,

Figure 1.5: Example of mobile radar equipment used for measurement of concrete structure. Original figure presented by Lai et al. (2011).

2004). An example of mobile radar equipment is shown in Figure 1.5. The basic principle and an example of a received radar signal are shown in Figure 1.6. The antenna sends an electromagnetic pulse towards the concrete plate. Due to change in dielectric constant (or "electromangetic impedance") reflections will occur. The antenna receives these reflections, and analyzes them with respect of amplitude and time delay. Radar is suitable for estimation of the location of reinforcement bars and cable ducts. Under favorable conditions (dry concrete) it is possible to detect reinforcement bars and cable ducts up to a distance of about 0.25-0.5 m from the surface (Shaw et al., 2004). Voids filled with air or water can also be detected using radar. The reflection from the back wall of e.g. a concrete plate create can be used to estimate relative thickness. For an exact estimation of thickness, a calibration or a known propagation velocity is needed.

Radar measurements can be performed very rapidly, which make the technique very suitable for creating images representing a cross section or volume of the object. An example of a measurement of such cross section and corresponding evaluation is shown in Figure 1.7.

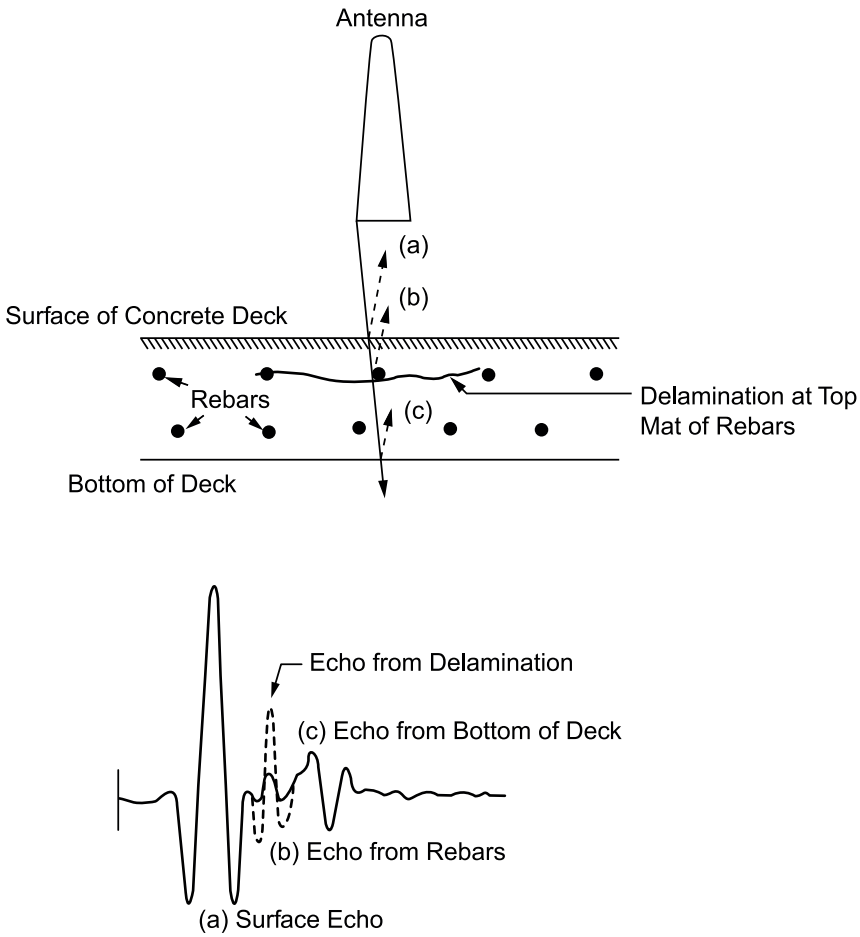

Figure 1.6: Sketch of principle for radar applied on a concrete deck (top part of figure), and simplified received signal (bottom part of figure). Original figure presented by Malhotra and Carino (2004)

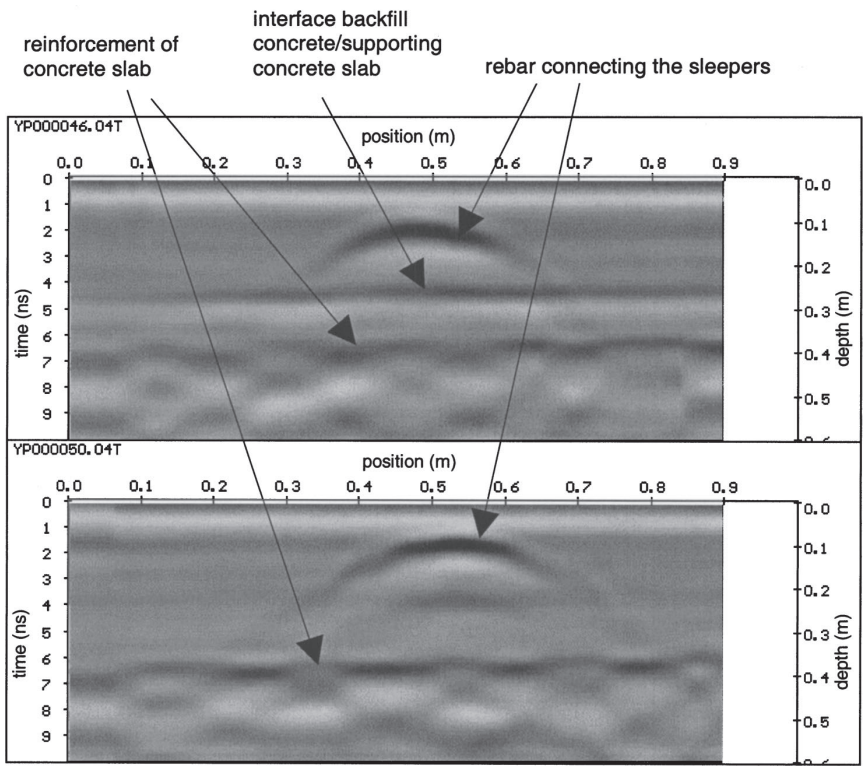

Figure 1.7: Example of imaging using radar on concrete. Original figure presented by Maierhofer (2003).

1.3 Acoustic methods

The term acoustic methods refer to techniques which are using mechanical wave propagation, i.e. "sound waves". Several techniques can be regarded as acoustic methods. Although the techniques are specialized and somewhat different, they are all using the same fundamental principle: the structural response/behavior (i.e. "sound") is dependent on the objects mechanical and geometric properties. By analyzing the response e.g. in the form of mechanical waves it is possible to extract information about the properties such as stiffness and dimensions of the structure.

1.3.1 Acoustic emission

Everyone has probably sometime noticed a cracking sound from e.g. a tree board under heavy load. The study of this type of sound generated by mechanical stress is the main idea of the acoustic emission technique. However, a permanent irreversible damage of the structure may have occurred when the sound was emitted, and from that point of view, acoustic emission is not always a truly non-destructive method. On the other hand, it is not necessarily the case that the ultimate limit state of the structure has been affected, even though a permanent damage may have occurred.

Although the basic principle of acoustic emission is very simple, the practical implementations are often extremely complicated. This is partly due to the fact that the mechanics of the "input force" (e.g. initiation of a crack) are in most cases unknown, or very complicated to describe. The interpretation of the observed "sound" may also be further complicated by the characteristics of the wave propagation in the structure (e.g. guided wave modes etc.).

Despite the difficulties of practical implementations of the acoustic emission technique, the benefits are often emphasized. Under the right circumstances it is possible to monitor a large partition of the structure. Thus, acoustic emission is often considered as a suitable option for structural health monitoring (SHM), which can be described as a permanently installed non-destructive technique performed continuously over time, i.e. monitoring.

1.3.2 Ultrasonic

The basic principle of ultrasonic techniques is more or less the same as for radar: a wave pulse is transmitted and the received signal is analyzed with respect to travel time and echoes. However, a main difference is

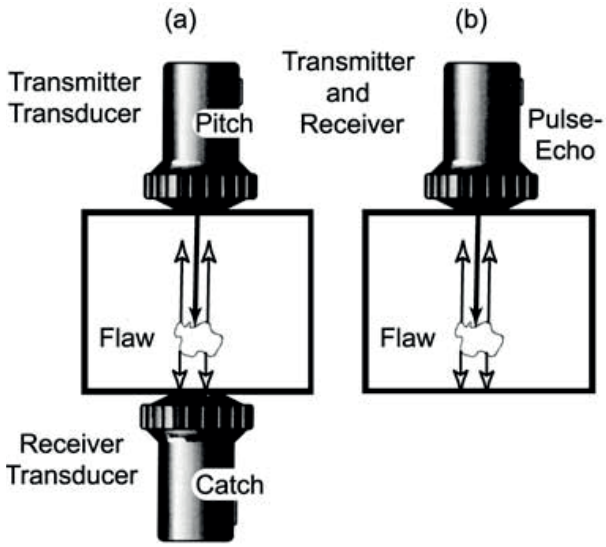

Figure 1.8: Measurement principle of pitch-catch technique (a), and pulse-echo technique. Original figure presented by Shull (2002).

that ultrasonic is based on mechanical wave propagation instead of electromagnetic wave propagation. Reflections are created when the propagating wave is influenced by changing material impedance (product of wave velocity and density), e.g. when the wave reaches a reinforcement bar. The time-delay of the echo indicate the location or origin of the impedance contrast.

Two main types of measurement set-ups for ultrasonic testing are the pitch-catch technique and the pulse echo technique. Figure 1.8 illustrates the principle of these two techniques. The pitch-catch technique is suitable for measuring the travel time i.e. velocity of the transmitted pulse. The pulse-echo technique is suitable for flaw detection, and is the only option if only one side of the structure is accessible.

Ultrasonic measurements are mainly using bulk waves. Two type of bulk waves exist in solid materials: the compression or longitudinal wave, and the shear or transversal wave. If the ultrasonic measurement is performed using wave propagation *along* the surface of an object, it is also possible to use Rayleigh waves or guided waves. Rayleigh waves are superposition of longitudinal waves and transversal waves, and exist due to the traction free boundary condition at the surface. Ultrasonic measurements are

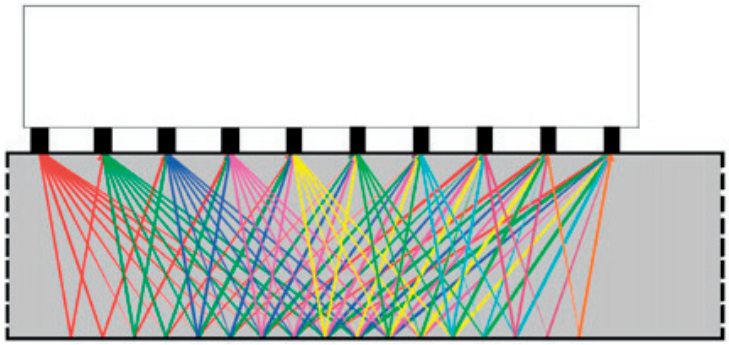

Figure 1.9: Example of measurement technique to create an image of a section of for example a concrete plate. Original figure presented by Shokouhi et al. (2014).

usually performed using frequencies in the interval 20 kHz to 500 kHz (Malhotra and Carino, 2004).

Ultrasonic measurements applied to concrete structures can be used to detect flaws, locate reinforcement bars, and measure thickness. Practical measurement is often performed as a continuous scan along a line, see Figure 1.9. Thus, it is possible to create an image representing the studied cross section, see Figure 1.10, where darker areas represents reflections/echoes with high relative amplitude (i.e. indicate a variation of impedance).

Depending on the wavelength (frequency) of the used pulse, the ultrasonic wave may be influenced by the heterogeneity of concrete. In fact, concrete consists of different materials: aggregate, binder (cement), and additives. This mixture of materials with different mechanical properties can disturb the ultrasonic wave, if the used wavelength is of the approximate same dimensions as the aggregates. Furthermore, the attenuation of ultrasonic waves is high in concrete. These two factors lead to several difficulties of using ultrasonic techniques on concrete , especially if the structure is thick and heavily reinforced.

1.3.3 Guided waves and Lamb waves

Pure bulk waves exists in infinite solid structures which have no boundaries. They can also exist in structures which can be *considered* as infinite compared to the wavelength of waves, i.e. they are approximated as infinite. However, when the wavelength becomes longer the influence from the structural boundaries will increase. At some point, the wavelength will

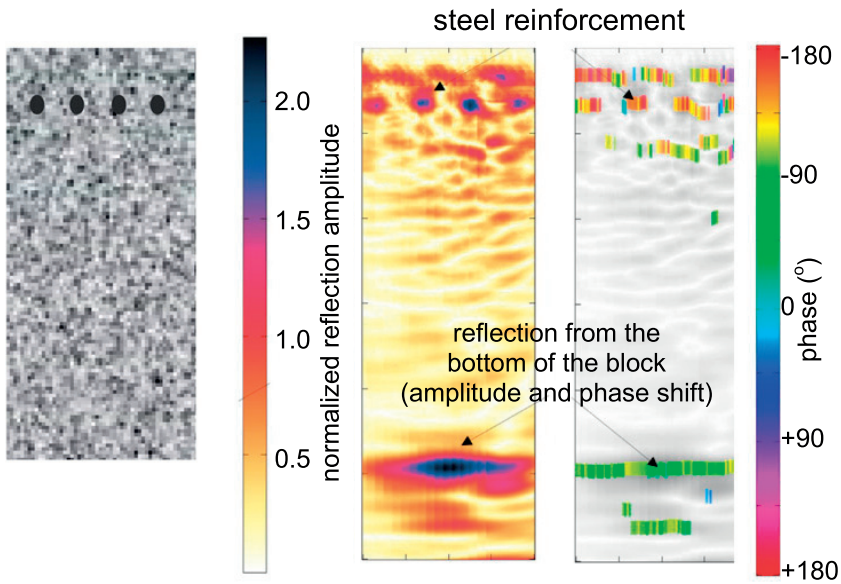

Figure 1.10: Example of result obtained from ultrasonic imaging measurement. Left part of figure shows cross-section with reinforcement, and right part of figure shows corresponding imaging results. Original figure presented by Shokouhi et al. (2014).

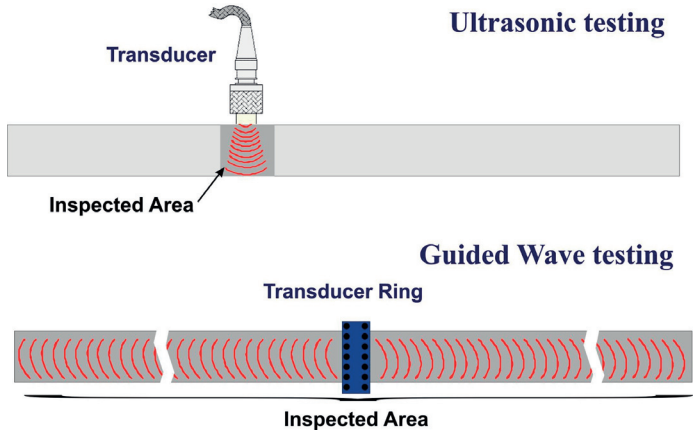

Figure 1.11: Difference between ultrasonic testing and guided wave testing. By using longer wavelengths, which become guided by the dimensions of the object, it is possible to increase the inspection range. Original figure by Sprialboy (licensed under CC BY-SA 3.0)

clearly be determined and affected by the boundaries of the structure. In such case, we have a guided wave, meaning that the actual wave is *guided* or defined by the structural boundaries. If the object is a plate, the wave is often referred to as a Lamb wave.

On one hand, guided waves can propagate over long distances, and for this reason, they are often used in non-destructive testing of objects where a long inspection range is of interest, e.g. testing of pipelines (Lowe et al., 1998). On the other hand, an increased inspection range often means that the resolution gradually decreases. Owing to this, guided wave testing does not replace local inspection techniques using e.g. ultrasonics, instead it is a complement which can for example be used to identify *approximately* where a flaw may exist. More locally performed measurements, for example by local ultrasonic testing, can thereafter be used to characterize the details of the possible flaw. A very simple comparison between ultrasonic testing and guided wave testing is shown in Figure 1.11.

Guided waves can be used as a non-destructive technique for concrete structures. Typically, the Lamb wave interpretation of a plate is used. One example of a method based on Lamb waves is the impact-echo method (Sansalone and Streett, 1997; Gibson and Popovics, 2005). An illustration of a practical impact-echo measurement combined with the utilized Lamb mode is shown in Figure 1.12. If the impact-echo method is combined with

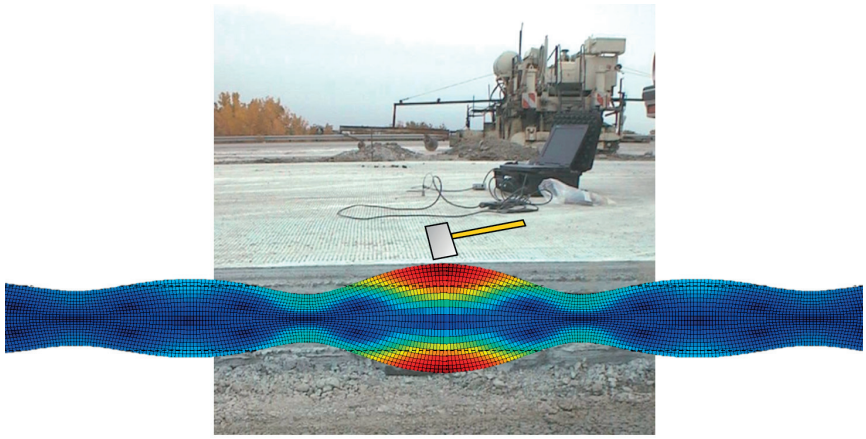

Figure 1.12: Impact-echo type of measurement using a hammer and an accelerometer. The first symmetric Lamb mode associated with the measurement is shown.

measurements of surface waves it is possible to estimate elastic material parameters (e.g. Young's modulus and Poisson's ratio) and thickness of plate-like concrete structures (Ryden et al., 2004). Impact-echo and similar techniques are particularly well suited for measurements on thick concrete structures, since the used wavelength is not influenced by scattering in the same way as for ultrasonic waves.

1.4 Motivation of work

Quantitative estimation of mechanical properties and thickness of concrete structures is important from a number of perspectives. It can for example serve as a verification of material quality, be used to monitor hardening, and can constitute important information in combined analysis such as data fusion, where different non-destructive techniques are evaluated simultaneously. The need for quantitative estimation of mechanical properties is predicted to increase in the future, for example due to demands stated by authorities working with safety issues concerning nuclear power plants.

Several activities are ongoing within the research topic of non-destructive testing of concrete structures. Substantial effort is directed toward imaging methods, i.e. measurement and processing techniques which create a visual representation of the studied material volume. Radiography, radar as well as ultrasonic techniques are particularly well suited for this type of application. Typically, images are used to detect voids and

cracks, locate reinforcement bars, etc. However, images do commonly visualize *relative* material variation of the volume, and are for this reason not very well suited for the task of *quantitative* non-destructive material characterization.

Ultrasonic techniques can be used to estimate acoustic wave velocities, which subsequently can be used to characterize the material. However, depending on aggregate size, reinforcement bars and thickness or dimensions of the object, ultrasonic measurements might be very complicated to perform with sufficient accuracy. The material condition associated with concrete, i.e. heterogeneity and high attenuation, is in fact, quite the opposite of the ideal condition of homogeneous material with low attenuation, e.g. steel. Thus, ultrasonic measurements on concrete are most relevant in the case of testing of core specimens with limited dimensions.

Evidently, there is a demand of non-destructive techniques, which are not based on ultrasonic wave propagation, for material characterization of concrete. Due to the nature of concrete materials it is clear that there is a potential in "low frequency" measurements using guided waves. This expected potential serve as a motivation for this PhD project to focus on further studies of the possibilities within combined impact-echo and surface wave measurements, i.e. approaches within the framework of guided waves or Lamb waves.

1.5 Aim and objective

The aim of this thesis, which is part of a PhD project that will result in a Doctoral thesis, is to study and develop techniques which can be used for material and structural characterization of plate-like concrete structures. The work is focused on a combined impact-echo and surface wave measurement along with evaluation techniques based on the theory of guided waves or Lamb waves.

The overall work within the PhD project is divided into the following steps:

Step I
: Study and evaluate the accuracy and reliability of existing techniques.

Step II
: Based on results from **Step I**, propose and develop new techniques.

1.6 Summary of appended papers

Paper I

O. Baggens and N. Ryden.
Systematic errors in Impact-Echo thickness estimation due to near field effects. NDT & E International, 69:16-27, Jan. 2015. ISSN 09638695. doi: 10.1016/j.ndteint.2014.09.003.

A systematic error which underestimates the plate thickness in impact-echo testing is studied. The study contains both numerical simulations and a practical field case. The systematic error is found to be dependent on the frequency of the pulse excitation, Poisson's ratio, and length of the measurement array. This type of error, which is dependent on distance to the pulse excitation source, is commonly referred to as near field effects. Numerical simulations indicate that the error due to near-field effects is approximately within a range of 5-15%. Estimation of the longitudinal wave velocity along the surface is found to be a major source of uncertainty in thickness estimations from impact-echo testing. This finding serves as a motivation for the work of developing alternative approaches for estimation of Poisson's ratio.

Paper II

O. Baggens and N. Ryden.
Poisson's ratio from polarization of zero-group velocity Lamb mode. Submitted for publication (Journal of the Acoustical Society of America). 2015.

A major conclusion from **Paper I** is that alternative approaches for estimation of Poisson's ratio is needed. For this reason, an alternative approach based on the polarization of the first symmetric zero-group velocity Lamb mode is proposed in **Paper II**. In this case, the polarization is interpreted as the ratio of the absolute amplitudes of the surface normal and surface in-plane components of the Lamb mode. A benefit from this approach, which is not dependent on the longitudinal wave velocity, is that an estimation of Poisson's ratio representative through the entire thickness of the plate is obtained. The proposed approach is demonstrated in a practical field case, where an increased accuracy of estimated nominal thickness is obtained compared with the conventional approach based on the longitudinal wave velocity.

Chapter 2

Related research

This chapter presents an overview of the related research within the field of non-destrutive evaluation of plate-like conrete structures.

2.1 Impact-echo method

Efficient non-destructive material characterization is important from several perspectives: e.g. quality control, maintenance, and safety (Maser, 2003; Deacon et al., 1997). The impact-echo method is one technique which has been proposed for non-destructive testing of concrete structures (Sansalone and Streett, 1997; Sansalone, 1997). The method is also standardized by the organization ASTM International (ASTM C 1383).

The following presentation will focus on the impact-echo method applied on concrete plates. However, note that this is not the only application of the impact-echo method. On the contrary, the general impact-echo type of measurement and its related basic physical principle (i.e. the study of a structural response) is not solely limited to plate-like structures. For example, impact-echo has been proposed as a non-destructive tool for structures such as columns, beams and pipes (Sansalone, 1997; Carino, 2001).

2.1.1 Assumed physical principle

The assumed physical principle of the impact-echo method, as proposed by Sansalone (1997), is shown in Figure 2.1. Figure 2.1 shows how a mechanical wave generated by an impact at the top surface will travel in a concrete plate which either contains a flaw (top subfigure (a)) or no flaw (bottom subfigure (b)). The same physical principle is also shown in Figure 2.2,

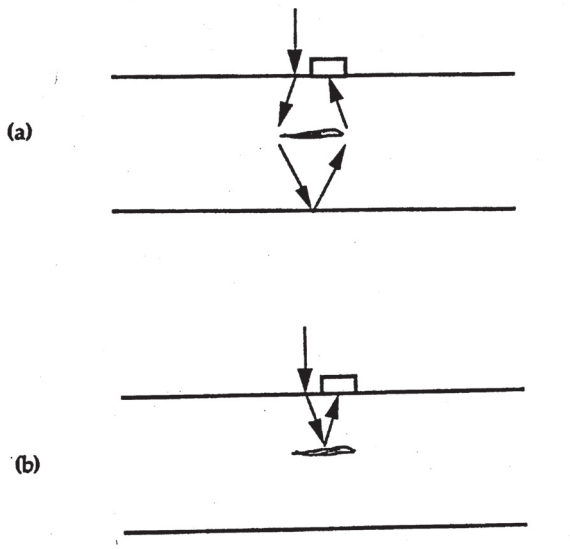

Figure 2.1: Assumed physical principle of the impact-echo method, as proposed by Sansalone (1997). The travel path for a mechanical wave is illustrated for a plate including a flaw (a), and a plate without a flaw (b). Original figure presented by Sansalone (1997).

which also shows an example of measurement equipment for impact-echo measurements. Depending of the length the wave has to travel up and down, see Figure 2.2, a variation in resonance frequency will occur. As a result, a shift in resonance frequency indicates a possible flaw. This type of measurement, where the *relative* shift of frequency is studied, is nowadays used on several concrete structures. The measurement is extremely simple and fast, and it is thereby possible to cover large areas efficiently.

The ray path or "bouncing wave" behavior as shown in Figure 2.1-2.2 has been suggested to be governed by the following *empirical* relation (Sansalone, 1997):

$$F_1 = \frac{\beta C_P}{2d} \tag{2.1}$$

where F_1 is the frequency of the first transient mode (i.e. the "thickness resonance"), β is a (correctional) factor describing the cross-sectional geometry, C_P is the longitudinal wave velocity, and d is the thickness of the object.

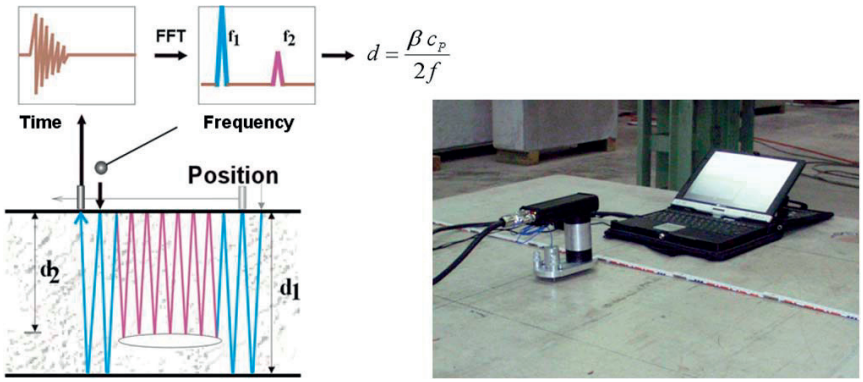

Figure 2.2: Assumed physical principle of impact-echo and example of measurement equipment. Original figure presented by Schubert and Köhler (2008)

2.1.2 Underestimated thickness

Eq. 2.1 provides a possibility to measure the thickness d of the studied object if F_1, β, and C_P are known. Typically, β is assumed depending of the object geometry. For plates, β is suggested to be equal to 0.96 (Sansalone, 1997). Early studies using the impact-echo method report accuracies of thickness estimation within 3 % (Sansalone and Streett, 1997). However, studies with more significant deviations exist (Popovics et al., 2006, 2008; Maser, 2003). In these studies the plate thickness is underestimated in 18 of 19 locations with a mean error of -8 %. Traditionally, this type of underestimated value of the thickness has been explained to be associated with an improper selection of value for the β factor.

2.1.3 Relation to Lamb waves

An important contribution to the understanding of the impact-echo method, and the *empirical* correctional factor β is given by Gibson and Popovics (2005). They demonstrate that the theoretically exact β factor is a function of Poisson's ratio. Furthermore, they manifest that the thickness resonance used in the impact-echo method corresponds to the minimum frequency of the first symmetric Lamb mode (S1), see Figure 2.3 and Figure 1.12. The group velocity for the S1 Lamb mode is zero at this minimum frequency, and for this reason, the mode is often abbreviated as S1-ZGV.

Zero-group velocity (ZGV) Lamb modes (Kausel, 2012; Prada et al., 2008) are used in other fields and applications which are not traditionally

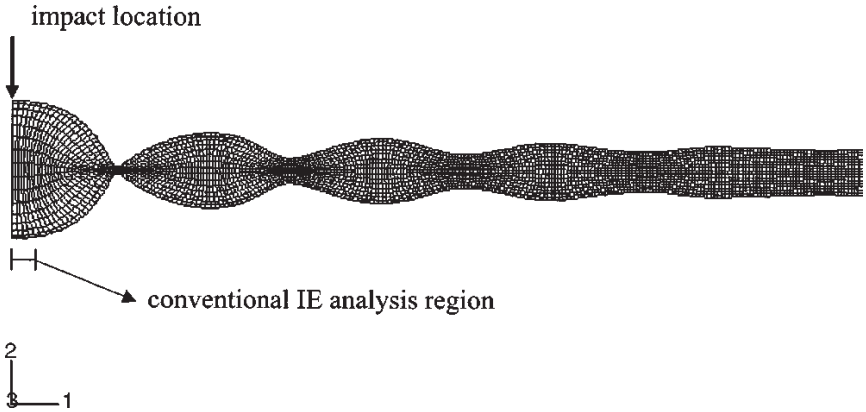

Figure 2.3: The impact-echo method employs the minimum frequency of the first symmetric (S1) Lamb mode, as illustrated in this figure. At this frequency, the group velocity is zero. Original figure presented by Gibson and Popovics (2005).

related to non-destructive testing of concrete. Some interesting and fascinating examples of applications are measurements of: acoustic bulk wave velocities and Poisson's ratio (Clorennec et al., 2007), thin-layer thickness (Cès et al., 2011), hollow cylinders (Cès et al., 2012), interfacial bond stiffness (Cheng et al., 2009), and air-coupled measurements (Holland and Chimenti, 2003).

It is evident that a major difference exist between the interpretation of the impact-echo method in Figure 2.1-2.2 and the Lamb wave interpretation in Figure 2.3 and Figure 1.12. Even though the Lamb wave interpretation nowadays is widely accepted, it is still not unusual to encounter the "ray-path" interpretation of the impact-echo method. Thus, the common misbelief which states that the impact-echo method is a point wise measurement rather than a measurement that is influenced by a major volume of the object (see Figure 2.3 and Figure 1.12) unfortunately still exists.

In Lamb wave theory a laterally infinite isotropic plate is defined by three independent parameters: e.g. the shear wave speed V_S, Poisson's ratio ν, and thickness h (Auld, 1990). In the case of measurements of an unknown plate thickness, the frequency of the S1-ZGV mode (i.e. the impact-echo frequency or the "thickness resonance frequency") must be complemented with an estimation of velocity (e.g. longitudinal, shear or Rayleigh), and Poisson's ratio to obtain the best possible estimation of the unknown thickness. In other words, non-destructive material

characterization based on the Lamb wave theory assumption requires that we have to measure at least three quantities, in order to characterize the plate.

2.2 Impact-echo and surface wave analysis

As mentioned previously, three parameters define a plate in Lamb wave theory. There exist different possibilities how these three parameters can be obtained. A common approach is to combine impact-echo with measurements of surface waves (Kim et al., 2006; Ryden and Park, 2006; Barnes and Trottier, 2009; Popovics et al., 2008). Although variations exist between these proposed techniques, the main idea is still the same. By use of relations which govern wave propagation and Lamb wave theory, the plate parameters (velocity, Poisson's ratio, and thickness) are obtained. The following presentation will focus on some different ideas and techniques which can possibly be used to solve this non-destructive characterization task. Associated difficulties related to these approaches are also presented.

2.2.1 Estimation of Poisson's ratio

A commonly used technique to determine Poisson's ratio is to measure the velocities of longitudinal wave and the Rayleigh wave (Wu et al., 1995), since the ratio between these two velocities is only dependent on Poisson's ratio. This technique is analog to determine Poisson's ratio from the ratio between the longitudinal wave velocity and shear wave velocity (Auld, 1990). It is clear that an accurate estimation of Poisson's ratio from this type of technique requires accurate estimations of velocities, and that the two velocities are measured over the same material volume.

Poisson's ratio can also be determined from the ratio between the frequency of the S1-ZGV Lamb mode and the minimum frequency of the second anti-symmetric Lamb mode (Clorennec et al., 2007). This approach has been demonstrated successfully for several thin homogenous metal plates (Clorennec et al., 2007), but only a few measurements have been reported for concrete plates (Gibson, 2004).

An alternative approach is based on the relation between the amplitude ratio between the surface in-plane and surface normal components of the Rayleigh wave (Bayon et al., 2005). However, to the author's knowledge, this approach has not been demonstrated on concrete plates. The ratio between the frequency of the S1-ZGV Lamb mode and the Rayleigh wave velocity can also be used to determine Poisson's ratio, but

this approach requires a known value of the thickness (Medina and Bayón, 2010).

2.2.2 Measurement of longitudinal wave velocity

The longitudinal wave velocity is usually estimated from the time taken by the first arriving wave from a transient impact to travel between two or multiple points separated by a known distance along the surface. A possible source of uncertainty in this type of analysis is the identification of a correct first arrival time. Unfortunately, identifying an accurate time point for the first arriving wave is not a trivial task, the displacement magnitude of the wave is typically very small.

Although the challenge of finding the first arriving wave, a commonly used procedure is to identify the first value above a certain threshold, and assume that this observed wave corresponds to a pure longitudinal wave. An alternative approach, which may facilitate the identification of the first arriving wave, is to study the trend of the measured signal instead of using a threshold level (Popovics et al., 1998).

Another challenge with measurements of the longitudinal wave velocity may occur if the material properties vary through the thickness. In such cases, the measured longitudinal wave velocity along the surface will be different from the longitudinal wave velocity measured through the plate. Gibson (2004) observed a systematic variation of this kind where an increased velocity was observed in measurements through the thickness of the plate compared with velocities obtained from measurements along the surface.

A material gradient with an increasing longitudinal wave velocity with depth has also been observed by (Popovics et al., 2006; Hu et al., 2006; Qixian and Bungey, 1996; Boyd and Ferraro, 2005). It has been suggested that a material gradient may be caused by a concentration of larger aggregates near the bottom of the slab during casting (Popovics et al., 2006). For this reason, Popovics et al. (2006) proposed a correction factor to compensate for the slower longitudinal wave velocity along the surface.

An alternative to a measurement of the longitudinal wave velocity from the first arriving wave, is to calculate the longitudinal wave velocity from the Rayleigh wave velocity (Kim et al., 2006). However, this approach requires an assumed or known value of Poisson's ratio.

2.2.3 Measurement of Rayleigh velocity

A simple technique to estimate the Rayleigh wave velocity is to study the cross correlation of two signals separated by a known distance (Wu et al., 1995). However, this technique may suffer from dispersion effects (Shin et al., 2007), and for this reason, the use of a continuous wavelet transform has been proposed. Another proposed approach for estimation of a Rayleigh wave velocity is the spectral analysis of surface waves method, SASW (Heisey et al., 1982). Recent approaches based on multichannel datsets (Ryden and Park, 2006; Barnes and Trottier, 2009) propose that the Rayleigh wave velocity can be estimated from the asymptotic trend of the fundamental Lamb modes in frequency-phase velocity domain (Park et al., 1999).

2.2.4 Measurement of S1-ZGV frequency

Ideal condition for impact-echo measurements exists in plates with infinite dimensions. In practical testing of concrete plates, this type of condition is rarely found, and we have to accept that the infinite plate condition cannot be fulfilled. As a consequence, the *finite* dimensions of the concrete plate can complicate the identification of the corresponding S1-ZGV frequency, since reflections of e.g. Rayleigh waves and other structural modes can exist.

Time frequency analysis is one approach which can enhance the identification of a correct S1-ZGV frequency (Abraham et al., 2000; Algernon and Wiggenhauser, 2007). Typically, combined impact-echo and surface wave measurements are based on multichannel recordings which are collected along the plate. Thus, it is possible to take use of the spatial distribution of the S1-ZGV mode. By summation of the signals in vicinity to the impact source the S1-ZGV frequency can be enhanced (Ryden and Park, 2006; Rydén, 2015). Another similar approach is based on a multiplication of several amplitude spectrums from signals measured close to the impact source (Medina and Garrido, 2007).

2.2.5 Uncertainties and issues

Several improvements have been proposed to the impact-echo method, among them the very important connecting link to Lamb wave theory (Gibson and Popovics, 2005). Thereby, from a Lamb wave point of view, it is theoretically possible to determine the exact plate thickness. However, a systematic error which underestimates the thickness in combined impact-echo and surface wave measurements appears to exist, see Table 2.1. Table 2.1 shows an underestimated thickness for the combined impact-echo and surface wave analysis technique, as well as the conventional

Test location		Estimated thickness (mm) and relative error (%)			
No	Thickness (mm)	Impact-echo (ASTM C1383)		Impact-echo and surface wave analysis (Lamb wave analysis)	
1	256	-		252	(-2%)
2	263	-		244	(-7%)
3	246	243	(-1%)	242	(-2%)
4	261	195	(-25%)	237	(-9%)
5	337	293	(-13%)	309	(-8%)
6	281	268	(-5%)	254	(-10%)
7	239	224	(-6%)	223	(-7%)

Table 2.1: Estimated thickness from impact-echo and combined impact-echo and surface wave analysis. Table created from data originally presented by Popovics et al. (2008).

impact-echo technique, in all test locations.

Baggens and Ryden (2015) reproduced this systematic error in numerical simulations and also observed the error in a practical measurement. A possible source to this systematic error is due to near-field effects caused by cylindrical spreading of waves from a point source and interference of different wave modes. Within the field of geophysics, near-field effects have been observed and studied for half-spaces (Zywicki and Rix, 2005; Roesset et al., 1990; Roesset, 1998; Bodet et al., 2009). However, for the case of non-destructive testing of plates, only a few studies have recognized the influence from the near-field of a point source (Ditri and Pilarski, 1994). In the context of impact-echo thickness testing of plates, near-field effects have traditionally not been taken into account (Baggens and Ryden, 2015).

A major uncertainty in measurements of impact-echo type is related to the estimation of a representative longitudinal wave velocity along the surface. This uncertainty clarifies the importance of finding alternative approaches for estimation of Poisson's ratio which are not dependent on the longitudinal wave velocity.

Chapter 3

Wave theory

This chapter presents some information about relevant theory of wave propagation.

3.1 Three dimensional infinite spaces

Two different type of mechanical waves can exist in three dimensional infinite spaces: the longitudinal wave, and transversal wave (Achenbach, 1973). These types of waves are also referred to as P-waves and S-waves, where the capital P and S represent **p**rimary or **p**ressure and **s**econdary or shear, respectively. The longitudinal wave velocity V_L is calculated according to:

$$V_L = \sqrt{\frac{E(1-v)}{\rho(1+v)(1-2v)}} \tag{3.1}$$

where E, v, ρ are the Young's modulus, Poisson's ratio and density, respectively. The transversal wave velocity V_T is calculated according to:

$$V_T = \sqrt{\frac{E}{2\rho(1+v)}} \tag{3.2}$$

The ratio between the longitudinal wave velocity and the transversal wave velocity is only dependent of Poisson's ratio and is given by:

$$\kappa = \frac{V_L}{V_T} = \sqrt{\frac{2(1-v)}{1-2v}} \tag{3.3}$$

The ratio κ is an important quantity, which provides a fundamental link between the acoustic bulk wave velocities V_L and V_T. The particle movements of plane longitudinal and transversal waves are shown in Figure 3.1.

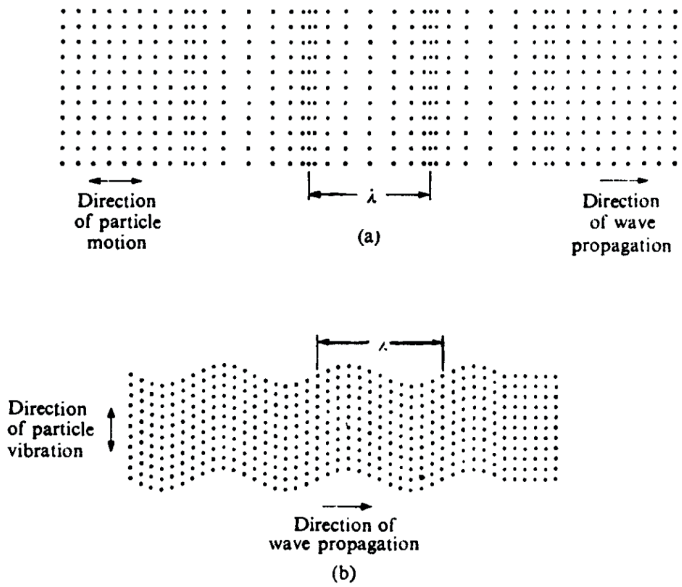

Figure 3.1: Illustration of particle motion for: (a) Longitudinal wave, (b) Transversal wave. Original figure presented by Graff (1975).

3.2 Half-spaces

A body which is infinite below a certain plane and non-existent above this plane is typically referred to as a half-space. The probably most common example of such semi-infinite body is the earth, which is almost infinite in the lateral/horizontal direction and depth, i.e. it is only limited by the earth surface if we assume a flat earth and ignore the curvature. However, structures which are similar to half-spaces can be found in many places, and it is typically the wavelength in comparison with the dimensions of the object that determines if an object can be assumed as infinite or not, rather than the specific dimensions of the object.

The free surface of the half-space makes it possible for surface waves to exist. Surface waves, which is often called Rayleigh waves, are created from combinations i.e. superposition of longitudinal and transversal waves. An example of a surface wave or Rayleigh wave is shown in Figure 3.2. Figure 3.2 shows that the displacement magnitude of the movement dominates at the surface.

The velocity of the Rayleigh wave cannot be determined in the same straightforward fashion as for the longitudinal and transversal wave.

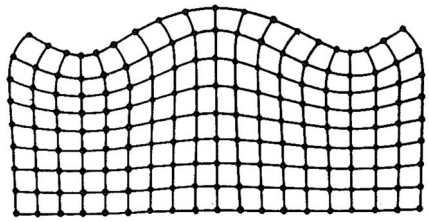

Figure 3.2: Rayleigh wave mode shape. Original figure presented by Viktorov (1967).

To determine the exact velocity, the so-called Rayleigh equation has to be solved (Viktorov, 1967). However, an approximation of the Rayleigh wave velocity can for example be determined from the relation given by (Achenbach, 1973):

$$\frac{V_R}{V_T} \approx \frac{0.862 + 1.14\nu}{1 + \nu} \tag{3.4}$$

3.3 Lamb waves

We have seen that two type of waves exist in an isotropic infinite body, and when a free surface exists (i.e. a half-space), Rayleigh waves can also exist. In the case of a plate, which has two free surfaces, additionally complexity is added to the wave propagation theory. This theory of wave propagation in linear elastic and laterally infinite plate is commonly referred to as Lamb wave theory.

The two free surfaces of the plate is equivalent to a traction free boundary condition, which means that the stress must equal zero at these surfaces. The boundary condition implicates that only certain combinations of longitudinal and transversal waves within the plate can exist at a given frequency. This means that only certain combinations of angular frequencies ω and lateral wave numbers k are possible. The valid combinations of frequencies ω and lateral wave numbers k, so-called ω-k pairs, define the dispersion characteristics of the plate, and can be obtained by solving the Lamb wave equation (Viktorov, 1967):

$$\frac{\tan(\beta h/2)}{\tan(\alpha h/2)} = -\left[\frac{4\alpha\beta k^2}{(k^2-\beta^2)^2}\right]^{\pm 1} \tag{3.5}$$

where

$$\alpha^2 = \omega^2/V_L^2 - k^2$$

$$\beta^2 = \omega^2/V_T^2 - k^2$$

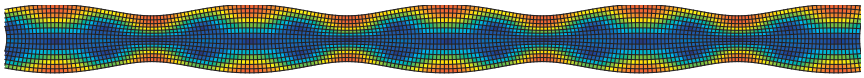

Figure 3.3: Example of symmetric Lamb mode.

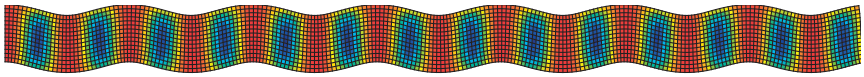

Figure 3.4: Example of anti-symmetric Lamb mode.

V_L and V_T are the longitudinal and transversal wave velocities, respectively, and h represents the plate thickness. The Lamb modes are divided into two main families: symmetric and anti-symmetric modes. The positive sign of the exponent on the right side of Eq. (3.5) defines symmetric modes, whereas the negative sign defines anti-symmetric modes. Examples of a symmetric and an anti-symmetric Lamb mode are shown in Figure 3.3 and Figure 3.4, respectively.

The valid ω-k pairs define the dispersive characteristics of the plate. The dispersion of Lamb waves contain important information which can for example be used to determine the elastic plate properties and thickness. The dispersion relations for a plate can be illustrated in many ways. One example is to plot the ω-k pairs for each Lamb mode directly, see Figure 3.5. Another possibility is to present the dispersion curves in the frequency-phase velocity domain, see Figure 3.6. The Rayleigh wave velocity can, for example, be determined by studying the convergence of the phase velocities for the A0 and the S0 modes, see Figure 3.6. The S1-ZGV point, which is the point of the minimum frequency of the S1-mode, is another quantity which can be determined. The frequency of this point corresponds to the thickness resonance used in traditional impact-echo measurements (Gibson and Popovics, 2005).

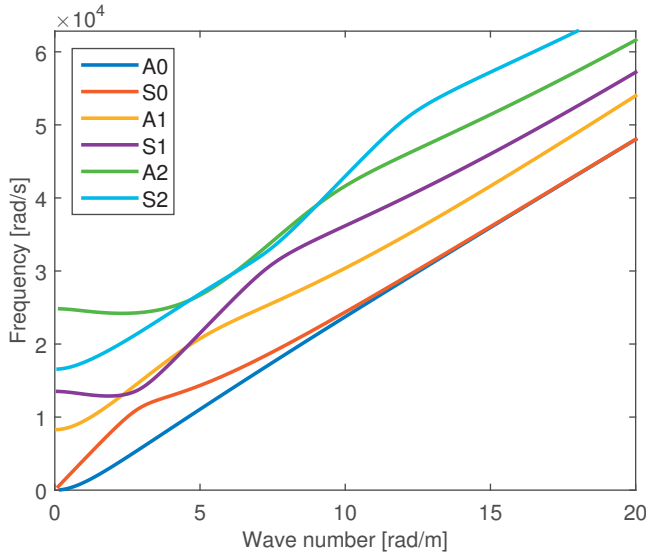

Figure 3.5: Dispersion curves (wave number-frequency plot) for a plate with Young's modulus 40 GPa, Poisson's ratio 0.2, density 2400 kg/m^3, and thickness 1 m.

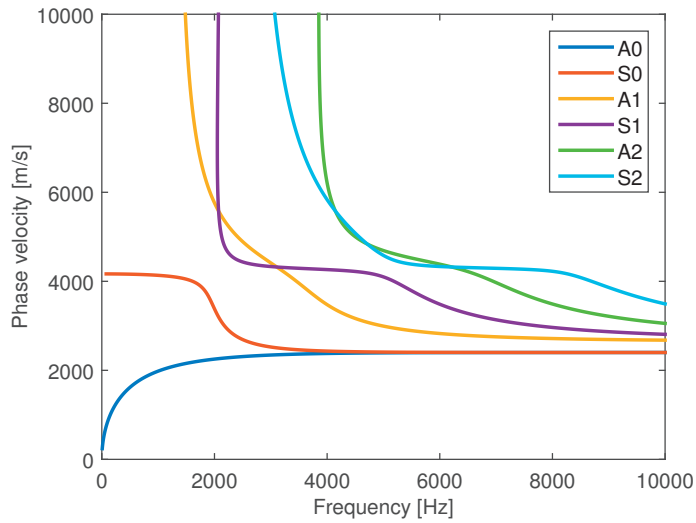

Figure 3.6: Dispersion curves (frequency-phase velocity plot) for a plate with Young's modulus 40 GPa, Poisson's ratio 0.2, density 2400 kg/m^3, and thickness 1 m.

Chapter 4

Numerical modeling

This chapter presents the basic theory of finite element modeling of dynamic problems, and demonstrates an implementation of a plate model in Comsol-Matlab.

4.1 Introduction to finite element theory

4.1.1 Equations of motion

To establish a finite element formulation we initially consider an arbitrary body subjected to a body force b_i $[\mathrm{N/m^3}]$ and a traction vector t_i $[\mathrm{N/m^3}]$ (Ottosen and Ristinmaa, 2005), see Figure 4.1. The subscript i represents the index $i = 1, 2, 3$, which denotes each coordinate axis. To fulfill Newton's second law, the following equation must be satisfied:

$$\int_S t_i \, dS + \int_V b_i \, dV = \int_V \rho \ddot{u}_i \, dV \tag{4.1}$$

where u_i is displacement, and ρ is density. In Eq. 4.1 the dot ($\dot{u}_i$) sign applied to u_i specifies differentiation with respect to time (i.e. $\dot{u}_i$ and $\ddot{u}_i$ represents velocity and acceleration, respectively). The traction vector t_i is given by:

$$t_i = \sigma_{ij} n_j \tag{4.2}$$

where σ_{ij} is a stress tensor. Insertion of Eq. 4.2 into Eq. 4.1 gives:

$$\int_S \sigma_{ij} n_j \, dS + \int_V b_i \, dV = \int_V \rho \ddot{u}_i \, dV$$

By use of Gauss divergence theorem, the surface integral can be transformed to a volume integral, and the following relation is obtained:

$$\int_V (\sigma_{ij,j} + b_i - \rho \ddot{u}_i) dV = 0$$

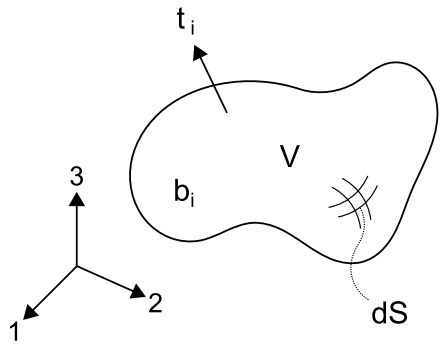

Figure 4.1: Arbitrary body subjected to the body force b_i, and traction vector t_i.

Since this relation should hold for arbitrary volumes it can be concluded that the following equations, "the equations of motion", must always be satisfied:

$$\sigma_{ij,j} + b_i = \rho \ddot{u}_i \tag{4.3}$$

4.1.2 Finite element formulation

The equations of motion (Eq. 4.3) describe an equilibrium relation at an infinitesimal point. This relation can be transformed into a so called weak formulation, which is a representation of the equations over a volume. It is done by multiplying Eq. 4.3 with an arbitrary *virtual* displacement field v_i and integrating over the volume:

$$\int_V v_i(\sigma_{ij,j} + b_i - \rho \ddot{u}_i) dV = 0$$

The word *virtual* emphasizes that the displacement field is a fictitious quantity, which is not the same as the *real/physical* displacement field. By use of the chain rule the expression is rewritten into:

$$\int_V [(\sigma_{ij} v_i)_{,j} - \sigma_{ij} v_{i,j}] dV + \int_V (v_i b_i - \rho v_i \ddot{u}_i) dV = 0 \tag{4.4}$$

With the Gauss theorem and Eq. 4.2, the following identity is established:

$$\int_V (\sigma_{ij} v_i)_{,j} dV = \int_S \sigma_{ij} v_i n_j dS = \int_S v_i t_i dS$$

which inserted into Eq. 4.4 gives:

$$\int_V \rho v_i \ddot{u}_i dV + \int_V v_{i,j} \sigma_{ij} dV = \int_V v_i t_i dS + \int_V v_i b_i dV \tag{4.5}$$

The small strain tensor ϵ_{ij} is given by:

$$\epsilon_{ij} = \frac{1}{2}(u_{i,j} + u_{j,i}) \tag{4.6}$$

where u_i is the displacement field of the body. By switching indices, it is evident that the small strain tensor is symmetric, i.e. $\epsilon_{ij} = \epsilon_{ji}$. It can also be shown that an analogous symmetry exists for the stress tensor as well, i.e. $\sigma_{ij} = \sigma_{ji}$. In Eq. 4.4, an arbitrary *virtual* displacement field was introduced and in a similar manner there is no restriction to introduce a *virtual* strain related to the *virtual* displacement field:

$$\epsilon^v_{ij} = \frac{1}{2}(v_{i,j} + v_{j,i}) \tag{4.7}$$

With Eq. 4.7, Eq. 4.5 becomes:

$$\int_V \rho v_i \ddot{u}_i \, dV + \int_V \epsilon^v_{ij} \sigma_{ij} \, dV = \int_V v_i t_i \, dS + \int_V v_i b_i \, dV \tag{4.8}$$

which is the weak form of the equations of motion.

The finite element method is a numerical tool which is practically implemented in computer code. It is therefore suitable to define some matrices which can be implemented with standard matrix operations. The following matrices are defined:

$$\epsilon^{\mathbf{v}} = \begin{bmatrix} \epsilon^v_{11} \\ \epsilon^v_{22} \\ \epsilon^v_{33} \\ 2\epsilon^v_{12} \\ 2\epsilon^v_{13} \\ 2\epsilon^v_{23} \end{bmatrix}; \quad \sigma = \begin{bmatrix} \sigma_{11} \\ \sigma_{22} \\ \sigma_{33} \\ \sigma_{12} \\ \sigma_{13} \\ \sigma_{23} \end{bmatrix}; \quad \ddot{\mathbf{u}} = \begin{bmatrix} \ddot{u}_1 \\ \ddot{u}_2 \\ \ddot{u}_3 \end{bmatrix}$$

$$\mathbf{v} = \begin{bmatrix} v_1 \\ v_2 \\ v_3 \end{bmatrix}; \quad \mathbf{t} = \begin{bmatrix} t_1 \\ t_2 \\ t_3 \end{bmatrix}; \quad \mathbf{b} = \begin{bmatrix} b_1 \\ b_2 \\ b_3 \end{bmatrix}$$

The objective is to create an approximation of the displacement field by interpolating values at node points with weight function, i.e. so called shape functions. The displacement field is approximated by the following expression:

$$\mathbf{u}(x_i, t) = \mathbf{N}(x_i)\mathbf{a}(t) \tag{4.9}$$

where $\mathbf{N}$ are the shape functions which approximate the values $\mathbf{a}$ at the nodal-points. The accelerations are approximated in a similar manner:

$$\ddot{\mathbf{u}}(x_i, t) = \mathbf{N}(x_i)\ddot{\mathbf{a}}(t) \tag{4.10}$$

A relationship between the displacements and the strain was given in Eq. 4.6. If the displacements are known it is obviously possible to determine the corresponding state of strain. The calculation of the strain can therefore be approximated by the following expression:

$$\epsilon = \mathbf{B}(x_i)\,\mathbf{a}(t) \tag{4.11}$$

where $\mathbf{B}$ are shape functions derived from differentiation of $\mathbf{N}$ according to Eq. 4.6.

In Eq. 4.8 a virtual displacement field v_i was introduced. In FEM a particular choice of the approximation of the virtual displacements is made according to the Galerkin method:

$$\mathbf{v} = \mathbf{N}\mathbf{c} \tag{4.12}$$

where c is vector containing arbitrary displacement values, which may be interpreted as arbitrary constants. In conformity with Eq. 4.11 the virtual strain is approximated by:

$$\epsilon^v = \mathbf{B}\mathbf{c}. \tag{4.13}$$

Going back to the virtual work expression in Eq. 4.8 and introducing the matrix formulations, we get the following expression:

$$\int_V \rho \mathbf{v}^T \ddot{\mathbf{u}} dV + \int_V \epsilon_v^T \sigma dV = \int_S \mathbf{v}^T \mathbf{t} dS + \int_V \mathbf{v}^T \mathbf{b} dV$$

By inserting Eq. 4.10, 4.12-4.13 the expression becomes:

$$\mathbf{c}^T \left\{ \int_V \rho \mathbf{N}^T \mathbf{N} dV \ddot{\mathbf{a}} + \int_V \mathbf{B}^T \sigma dV - \int_S \mathbf{N}^T \mathbf{t} dS - \int_V \mathbf{N}^T \mathbf{b} dV \right\} = 0.$$

As this expression should hold for any c, the following equations must always have to be fulfilled:

$$\int_V \rho \mathbf{N}^T \mathbf{N} dV \ddot{\mathbf{a}} + \int_V \mathbf{B}^T \sigma dV = \int_S \mathbf{N}^T \mathbf{t} dS + \int_V \mathbf{N}^T \mathbf{b} dV$$

Assuming that a constitutive relation which relates the stresses and the strains (e.g. Hooke's law in the case of linear elasticity) exists, and that this relation can be written (by use of Eq. 4.11) in the form of

$$\sigma = \mathbf{D}\epsilon = \mathbf{D}\mathbf{B}\mathbf{a}$$

we can finally write the finite element formulation:

$$\mathbf{M}\ddot{\mathbf{a}} + \mathbf{K}\mathbf{a} = \mathbf{f} \tag{4.14}$$

where

$$\mathbf{M} = \int_V \rho \mathbf{N}^T \mathbf{N} dV;\ \mathbf{K} = \int_V \mathbf{B}^T \mathbf{D} \mathbf{B} dV;\ \mathbf{f} = \int_S \mathbf{N}^T \mathbf{t} dS + \int_V \mathbf{N}^T \mathbf{b} dV$$

Equation 4.14 expresses a finite element formulation without any damping. However, it is possible to add a damping term:

$$\mathbf{M}\ddot{\mathbf{a}} + \mathbf{C}\dot{\mathbf{a}} + \mathbf{K}\mathbf{a} = \mathbf{f} \tag{4.15}$$

which is the finite element formulation with damping described by the matrix $\mathbf{C}$.

4.1.3 Response to harmonic excitation

A system represented by the finite element formulation Eq. 4.15 subjected to a harmonic force with the amplitude $\mathbf{f}_0$ and the angular frequency $\omega = 2\pi f$ can be described by:

$$\mathbf{M}\ddot{\mathbf{u}} + \mathbf{C}\dot{\mathbf{u}} + \mathbf{K}\mathbf{u} = \mathbf{f}_0 e^{i\omega t} \tag{4.16}$$

It can be shown that the response of the displacement field $\mathbf{u}$ is periodic with the same frequency ω as the excitation force. The displacement field $\mathbf{u}$ may then be described by:

$$\mathbf{u} = \mathbf{u}_0 e^{i\omega t}$$

where $\mathbf{u}_0$ is a complex amplitude. Differentiation of $\mathbf{u}$ yield:

$$\dot{\mathbf{u}} = i\omega \mathbf{u}_0 e^{i\omega t};\ \ddot{\mathbf{u}} = -\omega^2 \mathbf{u}_0 e^{i\omega t}$$

Insertion into Eq. 4.16 gives:

$$(-\omega^2 \mathbf{M} + i\omega \mathbf{C} + \mathbf{K})\mathbf{u}_0 = \mathbf{f}_0 \tag{4.17}$$

which is a system of equations completely independent of time. As a result, this system can be solved entirely with algebraic methods. Result obtained from this type of analyses is extremely useful. It provide important knowledge about the structural response as function of frequencies. Thus, the time domain response to an arbitrary pulse excitation can be obtained using Fourier analysis. This will be demonstrated in the following section.

4.2 Finite element modeling in Comsol and Matlab

The finite element software Comsol and the computational software Matlab was used to perform simulations of wave propagation in plates. The following presentation will focus on the implementation of a finite

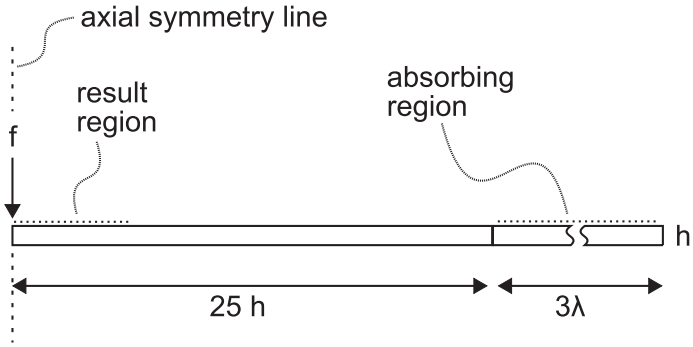

Figure 4.2: Sketch of plate model.

element model which simulates the response of a plate subjected to transient impacts. This implementation is mainly based on the modeling techniques presented by Castaings et al. (2004); Hosten and Castaings (2006); Ryden and Castaings (2009).

An example of an axially symmetric plate model is shown in Figure 4.2. A load is applied at the axial symmetry axis to simulate the point load. The plate is divided into two main regions: result region and absorbing region. The response is extracted from the result region whereas the absorbing region is used to simulate infinite boundaries of the plate. The absorbing region is created by using a gradually increasing damping ratio (Castaings et al., 2004).

The model was solved in frequency domain using an element mesh and absorbing region which were adjusted to the frequency. At low frequencies a coarse mesh was used, as opposed to the case of high frequencies where a fine mesh was used (Ryden and Castaings, 2009). The absorbing region was adjusted for each frequency to be equal to the length of three times the longitudinal wave length at the studied frequency. The response of the plate in terms of complex amplitudes, i.e. so-called transfer functions, was extracted from the result region of the plate, see Figure 4.2. An example of the absolute amplitude of a transfer function is plotted in Figure 4.3.

Force excitation pulses, which were applied at the axial symmetric axis to simulate a point load (see Figure 4.2), were defined from a Gaussian mono-pulse. An example of a force excitation pulse is shown in Figure 4.4. Time domain responses were obtained from the inverse discrete Fourier transforms of the transfer functions multiplied with the frequency spectrum of the pulses (Castaings et al., 2004). An example of dataset in time domain is shown in Figure 4.5. An overview of the used modeling

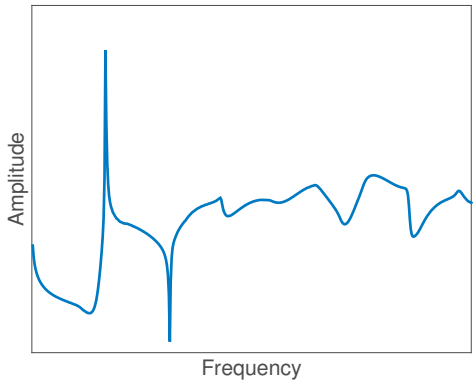

Figure 4.3: Example of the absolute value of transfer function.

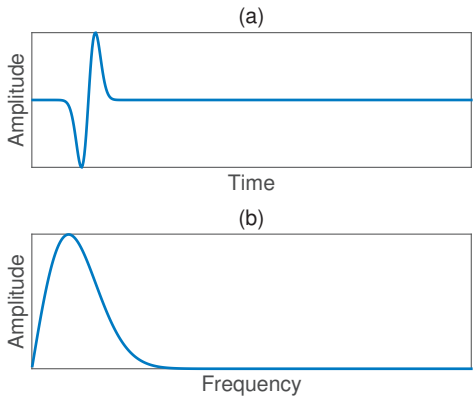

Figure 4.4: Force exciation pulse in (a) Time domain, (b) Frequency domain.

technique is shown in Figure 4.6.

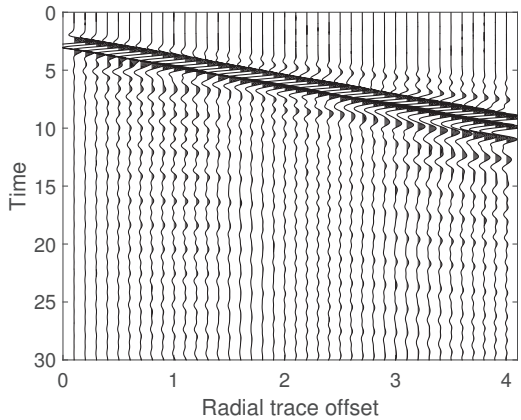

Figure 4.5: Time domain dataset.

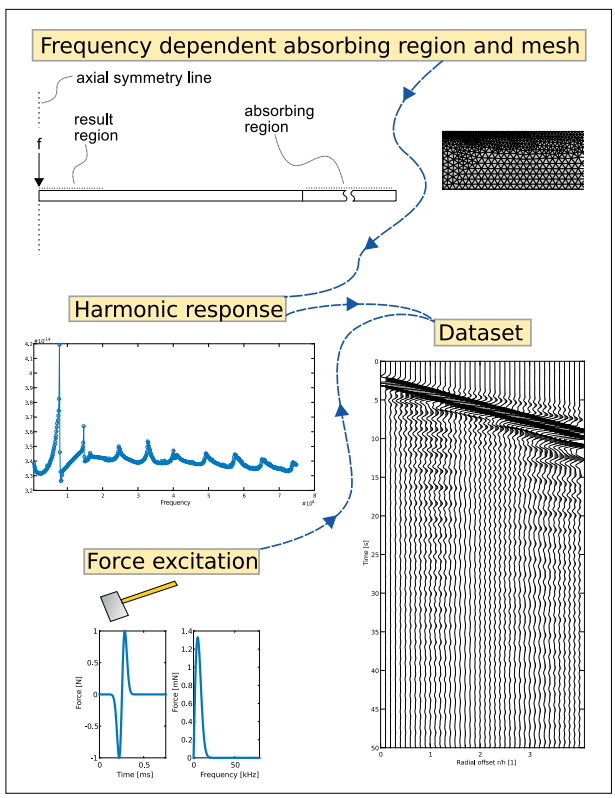

Figure 4.6: Overview of modeling technique.

Chapter 5

Measurement technique

This chapter presents the measurement equipment and techniqe used in the practical field cases.

Practical measurements have been performed on concrete plates with a hammer as an impactor and an accelerometer as a receiver. Typically, several hammer impacts have been performed at an increasing offset distance from the accelerometer, which have been attached at a fixed position. The structural response in terms of acceleration has been recorded by the accelerometer, as well as the time history of the impact-force from the hammer. By using the reciprocity theorem for linear elastic system a multichannel dataset can be created. This type of dataset is typical for a combined impact-echo and surface wave analysis. A sketch illustrating the practical measurement techniques and procedure is shown in Figure 5.1.

The measurement equipment consists of an impact-hammer, accelerom-

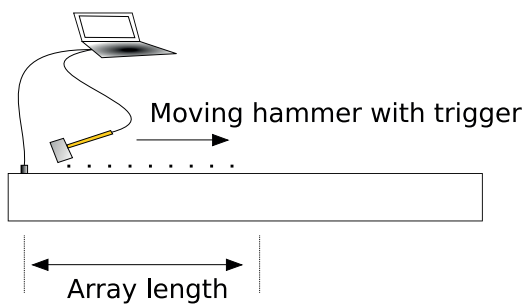

Figure 5.1: Sketch of measurement technique.

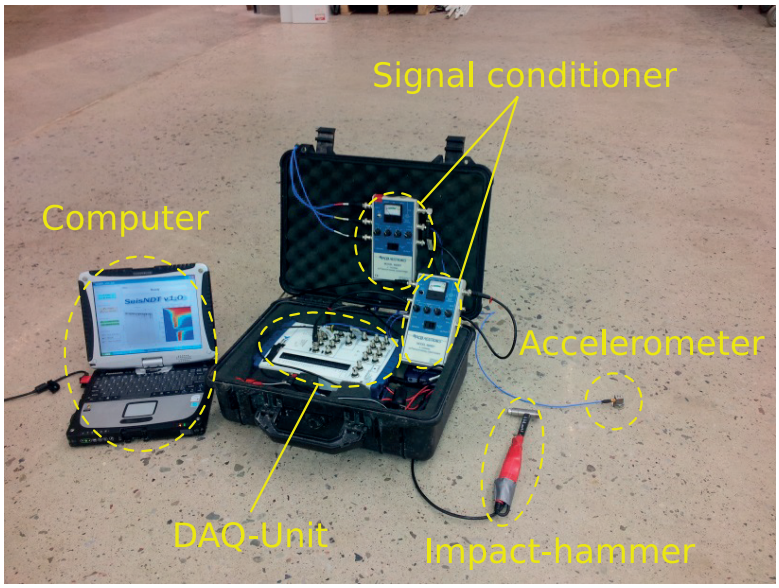

Figure 5.2: Measurement equipment: impact-hammer (PCB model 086C03), accelerometer (PCB model 339A30), signal conditioner (PCB model 480b21), DAQ-unit (NI USB-6251 BNC), and computer (Panasonic Toughbook).

eter, signal conditioner, DAQ-unit, and a computer. An overview of the measurement equipment is shown in Figure 5.2. Figure 5.3 shows an example of a three component accelerometer . As seen, this is a very portable and flexible system in which every individual part of equipment easily can be changed or replaced. For example, it is common to select impactor with respect to the object that is studied. If a thick structure is considered it is suitable to use a heavy impactor which can generate sufficient low frequencies in the impact pulse. On the contrary, if a thin structure is considered it is suitable to use a light impactor which can generate sufficient high frequencies in the impact. An example of different impactors is shown in Figure 5.4.

Figure 5.3: Three component accelerometer (PCB model 339A30).

Figure 5.4: Impact hammers, from left: home-made impactor (screw/bolt) with piezoelectric crystal, hammer PCB model 086C03, hammer PCB model 086D05.

Chapter 6

Main results and future research

This chapter presents the main results from the papers and possibilites for future research.

6.1 Main results

Three parameters, e.g. velocity, Poisson's ratio, and thickness, define a plate in Lamb wave theory. In combined impact-echo and surface wave analysis, this theory can be used to estimate the elastic properties and thickness of a plate. Figure 6.1 (a) shows a selection of the dispersion curves (Lamb modes A0, S0, A1, and S1) for a plate with $\nu = 0.2$. The axes are normalized with the thickness h and the transversal wave speed V_S. This normalization makes the curves only dependent on ν, i.e. they are valid for all plates with $\nu = 0.2$. The S1-ZGV point, which represents the Lamb mode used in impact-echo measurements, is also plotted. By studying this type of Lamb wave dispersion curves of a plate, the theoretical foundation for the evaluation of the elastic properties and thickness can easily be illustrated and explained.

Figure 6.1 (b) shows an expanded view of the S1-ZGV points for different values of ν. The normalization of the axes makes the variations of the locations for the S1-ZGV points to be only dependent on ν. This implies that the value of fh/V_S (i.e. x-axis) for the S1-ZGV point is constant for a fixed value of ν. Thus, fh/V_S provides a direct way of determining the plate thickness once V_S, ν, and f are known.

Results from the literature review indicate a systematic error in terms of underestimated thickness from impact-echo thickness testing. Underestimated velocities is one possible source of error leading to an

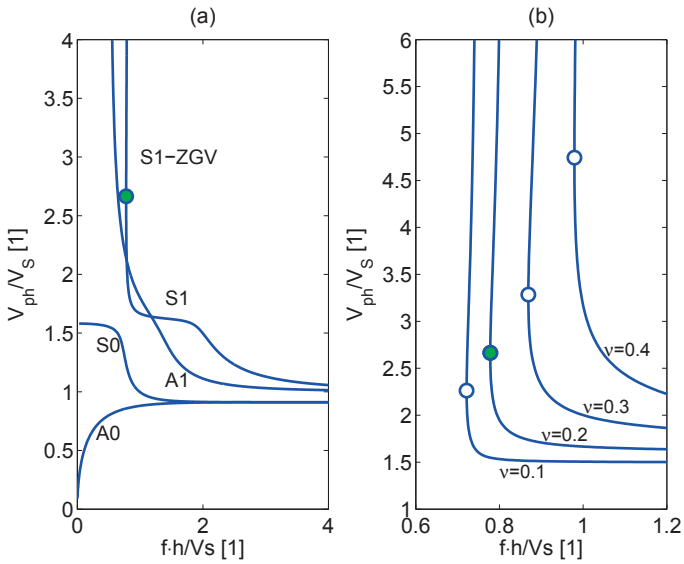

Figure 6.1: (a) Lamb wave dispersion curves (A0, S0, A1, and S1 mode) for a plate with $\nu = 0.2$. (b) Expanded view around S1-ZGV points for different values of Poisson's ratio.

underestimated thickness. Detailed numerical simulations show that there exists a zone, close to the impact source (see Figure 6.2 (b)), where the velocity of the first arriving wave cannot be directly linked to the theoretical longitudinal wave velocity. This zone, where the high amplitude of the Rayleigh wave hides the longitudinal wave, results in an underestimated velocity, which in turn, leads to an uncertain estimation of Poisson's ratio and an underestimated thickness. The magnitude of underestimated thickness is dependent on Poisson's ratio, pulse frequency content, and the distance between the measurement and the impact source. A more thorough analysis of the near-field effects is given in **Paper I**.

Figure 6.3 (a) and Figure 6.3 (b) show the variation of estimated first arrival velocity for a combined impact-echo and surface wave measurement and the conventional impact-echo method, respectively. It can be seen that the estimated first arrival velocity is clearly affected by the near field. These results verify the inherently difficult and questionable task of estimating the longitudinal wave velocity from first arrivals of dispersive Lamb waves. For this reason, an alternative approach for estimation of Poisson's ratio is proposed.

The details of this novel approach for estimation of Poisson's ratio is

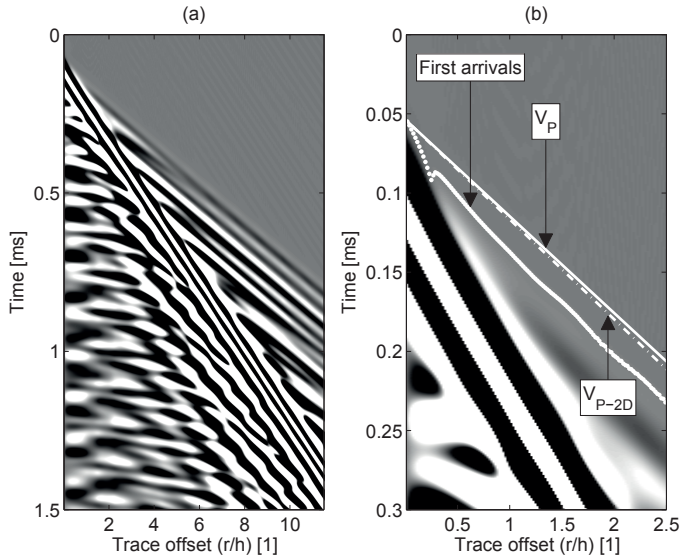

Figure 6.2: (a) Detailed finite element simulation of impact-echo and surface wave test. (b) Expanded view close to impact source showing traces/signals within a radial distance of $2.5 \cdot r/h$.

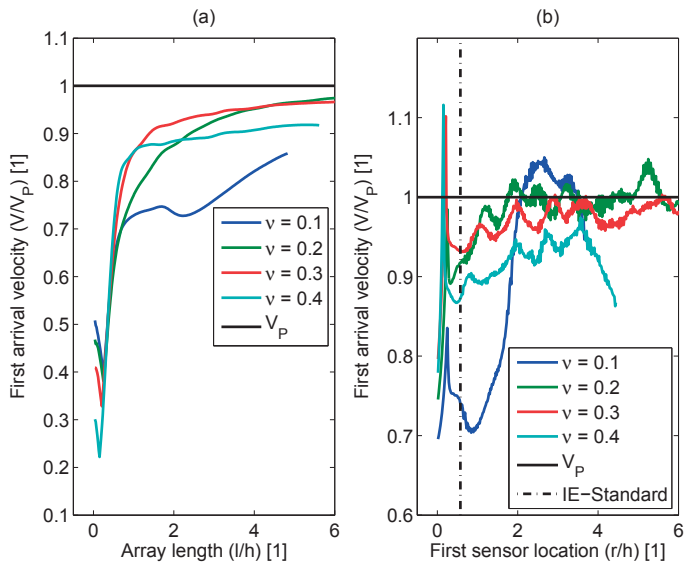

Figure 6.3: Estimated first arrival velocity using a combined impact-echo and surface wave measurement (a), and the conventional impact-echo method (b).

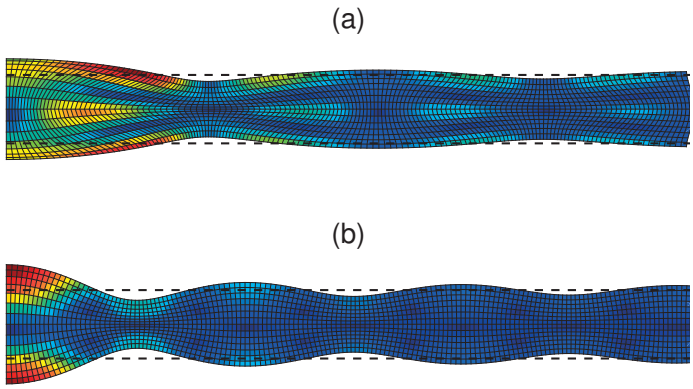

Figure 6.4: Mode shape, with cylindrical spreading due to a point load, of first symmetric zero-group velocity Lamb mode (S1-ZGV): (a) $\nu = 0.4$, (b) $\nu = 0.2$.

presented in **Paper II**. The proposed approach is not dependent on a longitudinal wave velocity. Instead, it is based on the amplitude polarization of the first symmetric zero-group velocity Lamb mode (S1-ZGV). In this case, the amplitude polarization is interpreted as the ratio between the amplitude of the surface normal component and the amplitude of the surface in-plane component.

The main idea of this new approach is illustrated in Figure 6.4. For high Poisson's ratio, the movement of the mode shape is dominated by the surface in-plane component, see Figure 6.4 (a), whereas for low Poisson's ratio, the movement is dominated by the surface normal component, see Figure 6.4 (b). This variation of polarization of the mode shape can be used to determine Poisson's ratio in practical measurements. An advantage of this approach is that a through-thickness representative estimation of Poisson's ratio is obtained, since the used Lamb mode exists through the entire thickness of the plate.

A demonstration of this approach applied on data collected in a practical field case is shown in Figure 6.5. Figure 6.5 shows the absolute amplitude of the measured first symmetric zero-group velocity Lamb mode (markers). A best match between the extracted mode shape (markers) and the theoretical mode shape (lines) is determined. From this best match the polarization is calculated, and thereby, an estimation of Poisson's ratio is obtained. In this practical field case an increased accuracy in estimated nominal thickness is obtained compared with the results using the traditional approach based on a longitudinal wave velocity.

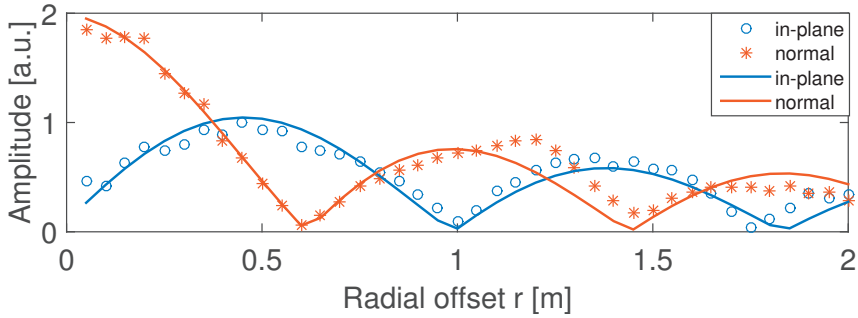

Figure 6.5: Measured mode shape (markers) of first symmetric zero-group velocity Lamb mode (S1-ZGV), and best match (lines).

6.2 Future research

Based on results from the literature review, **Paper I**, and **Paper II**, the following general topics represents possible and interesting ideas for future research:

Material gradients

Results from the literature review show that material gradients with varying stiffness through the thickness can exist. By using Lamb wave theory this possible material gradient is ignored, since a plate in Lamb wave theory is isotropic. Thus, an idea for future research is to study plates with material gradients, e.g. an increasing stiffness with depth of the plate.

Defects

Future research can also focus on the possibilities and limitations of detecting *abrupt* material conditions through the thickness caused by e.g. delaminations. For example reactor containment walls in nuclear power plants often consist of a steel liner embedded in concrete. To ensure operational safety of the plant, it is important that the steel liner is intact. It is often assumed that a debonded steel liner can indicate a possible defect like corrosion. Thus, this bonding condition is of interest to verify with non-destructive methods. For the case of containment walls in nuclear power plants, it is also of interest to study the possible influence from the curvature of the wall.

2D Arrays

The practical measurements have been carried out by performing hammer impacts along a straight line, i.e. an array in one dimension has been used. To increase the quality of the measured data, and

also open up for new possibilities in terms of more detailed evaluation, a possible research topic is alternative measurement arrays, e.g. a two-dimensional array (i.e. grid) can be studied.

Data evaluation

If data is collected using a 2D array, and is combined with more refined signal processing, it is likely that additional features (e.g. higher Lamb modes such as A2-ZGV etc.) can be used to enhance the data evaluation. Future research within this topic is important to enable a further development of the infinite plate model towards gradually more complicated objects and boundary conditions.

Bibliography

O. Abraham, C. Leonard, P. Cote, and B. Piwakowski. Time frequency analysis of impact-echo signals: numerical modeling and experimental validation. *ACI Materials journal*, (97):645–657, 2000. doi: 10.14359/9978.

J. D. Achenbach. *Wave Propagation in Elastic Solids*. North-Holland Publishing Company, 1973.

D. Algernon and H. Wiggenhauser. Impact Echo Data Analysis Based on Hilbert-Huang Transform. *Transportation Research Record*, 2028(-1): 146–153, Dec. 2007. ISSN 0361-1981. doi: 10.3141/2028-16.

ASTM C 1383. Standard Test Method for Measuring the P-Wave Speed and the Thickness of Concrete Plates Using the Impact-Echo Method, Annual Book of American Society for Testing and Materials (ASTM) Standards.

B. Auld. *Acoustic Fields and Waves in Solids, Vol. II*. Robert E. Krieger Publishing Company, Malabar, Florida, 2nd edition, 1990.

O. Baggens and N. Ryden. Systematic errors in Impact-Echo thickness estimation due to near field effects. *NDT & E International*, 69:16–27, Jan. 2015. ISSN 09638695. doi: 10.1016/j.ndteint.2014.09.003.

C. L. Barnes and J.-F. Trottier. Hybrid analysis of surface wavefield data from Portland cement and asphalt concrete plates. *NDT & E International*, 42(2):106–112, Mar. 2009. ISSN 09638695. doi: 10.1016/j.ndteint.2008.10.003.

A. Bayon, F. Gascon, and F. J. Nieves. Estimation of dynamic elastic constants from the amplitude and velocity of Rayleigh waves. *The Journal of the Acoustical Society of America*, 117(6):3469, 2005. ISSN 00014966. doi: 10.1121/1.1898663.

L. Bodet, O. Abraham, and D. Clorennec. Near-offset effects on Rayleigh-wave dispersion measurements: Physical modeling. *Journal of Ap-*

plied Geophysics, 68(1):95–103, May 2009. ISSN 09269851. doi: 10.1016/j.jappgeo.2009.02.012.

A. Boyd and C. Ferraro. Effect of curing and deterioration on stress wave velocities in concrete. *Journal of materials in civil engineering*, (April): 153–158, 2005. doi: 10.1061/(ASCE)0899-1561(2005)17:2(153).

N. Carino. The impact-echo method: an overview. *Proceedings of the 2001 Structures Congress & Exposition*, page 18, 2001. doi: 10.1061/40558(2001)15.

M. Castaings, P. Cawley, R. Farlow, and G. Hayward. Single Sided Inspection of Composite Materials Using Air Coupled Ultrasound. *Journal of Nondestructive Evaluation*, 17(1):37–45, 1998. ISSN 1573-4862. doi: 10.1023/A:1022632513303.

M. Castaings, C. Bacon, B. Hosten, and M. V. Predoi. Finite element predictions for the dynamic response of thermo-viscoelastic material structures. *The Journal of the Acoustical Society of America*, 115(3):1125, 2004. ISSN 00014966. doi: 10.1121/1.1639332.

M. Cès, D. Clorennec, D. Royer, and C. Prada. Thin layer thickness measurements by zero group velocity Lamb mode resonances. *The Review of scientific instruments*, 82(11):114902, Nov. 2011. ISSN 1089-7623. doi: 10.1063/1.3660182.

M. Cès, D. Royer, and C. Prada. Characterization of mechanical properties of a hollow cylinder with zero group velocity Lamb modes. *The Journal of the Acoustical Society of America*, 132(1):180–5, July 2012. ISSN 1520-8524. doi: 10.1121/1.4726033.

C.-C. Cheng, C.-P. Yu, and T. Liou. Evaluation of interfacial bond condition between concrete plate-like structure and substrate using the simulated transfer function derived by IE. *NDT & E International*, 42(8):678–689, Dec. 2009. ISSN 09638695. doi: 10.1016/j.ndteint.2009.06.001.

D. Clorennec, C. Prada, and D. Royer. Local and noncontact measurements of bulk acoustic wave velocities in thin isotropic plates and shells using zero group velocity Lamb modes. *Journal of Applied Physics*, 101(3): 034908, 2007. ISSN 00218979. doi: 10.1063/1.2434824.

J. A. Deacon, C. L. Monismith, and J. T. Harvey. Pay Factors for Asphalt-Concrete Construction: Effect of Construction Quality on Agency Costs. Technical report, Pavement Research Center, Institute of Transportation Studies, University of California, Berkeley, 1997.

J. Ditri and A. Pilarski. Generation of guided waves in a plate by axisymmetric normal surface loading. *Review of Progress in Quantitative Nondestructive Evaluation*, 13, 1994.

A. Gibson. *Advances in Nondestructive Testing of Concrete Pavements*. Ph.d. thesis, University of Illinois, 2004.

A. Gibson and J. Popovics. Lamb wave basis for impact-echo method analysis. *Journal of Engineering mechanics*, pages 1–6, 2005. doi: 10.1061/(ASCE)0733-9399(2005)131:4(438).

K. F. Graff. *Wave Motion in Elastic Solids*. Dover Publications, New York, 1975. ISBN 0-486-66745-6.

J. S. Heisey, K. H. Stokoe, and A. H. Meyer. Moduli of pavement systems from spectral analysis of surface waves. Technical report, Transportation Research Record 852, Transportation Research Board, Washington, D.C., 1982.

S. D. Holland and D. E. Chimenti. Air-coupled acoustic imaging with zero-group-velocity Lamb modes. *Applied Physics Letters*, 83(13):2704, 2003. ISSN 00036951. doi: 10.1063/1.1613046.

B. Hosten and M. Castaings. FE modeling of Lamb mode diffraction by defects in anisotropic viscoelastic plates. *NDT & E International*, 39(3):195–204, Apr. 2006. ISSN 09638695. doi: 10.1016/j.ndteint.2005.07.006.

M. Hu, Y. Lin, and C. Cheng. Method for Determining Internal P-Wave Speed and Thickness of Concrete Plates. *ACI Materials Journal*, 103(5):327–335, 2006. ISSN 0889-325X. doi: 10.14359/18154.

E. Kausel. Number and location of zero-group-velocity modes. *The Journal of the Acoustical Society of America*, 131(5):3601–10, May 2012. ISSN 1520-8524. doi: 10.1121/1.3695398.

D. Kim, W. Seo, and K. Lee. IE-SASW method for nondestructive evaluation of concrete structure. *NDT & E International*, 39(2):143–154, Mar. 2006. ISSN 09638695. doi: 10.1016/j.ndteint.2005.06.009.

W. L. Lai, T. Kind, and H. Wiggenhauser. NDT & E International Using ground penetrating radar and time-frequency analysis to characterize construction materials. *NDT and E International*, 44(1):111–120, 2011. ISSN 0963-8695. doi: 10.1016/j.ndteint.2010.10.002.

M. Lowe, D. Alleyne, and P. Cawley. Defect detection in pipes using guided waves. *Ultrasonics*, 36(1-5):147–154, Feb. 1998. ISSN 0041624X. doi: 10.1016/S0041-624X(97)00038-3.

C. Maierhofer. Nondestructive Evaluation of Concrete Infrastructure with Ground Penetrating Radar. *Journal of Materials in Civil Engineering*, 15 (June):287–297, 2003. ISSN 0899-1561. doi: 10.1061/(ASCE)0899-1561(2003)15:3(287).

V. Malhotra and N. Carino. *Handbook on Nondestructive Testing of Concrete*. CRC Press, Boca Raton, Florida, 2nd edition, 2004. ISBN 0-8493-1485-2.

K. R. Maser. Non-Destructive Measurement of Pavement Layer Thickness. *Final Report Caltrans No. 65A0074*, 2003.

R. Medina and A. Bayón. Elastic constants of a plate from impact-echo resonance and Rayleigh wave velocity. *Journal of Sound and Vibration*, 329(11):2114–2126, May 2010. ISSN 0022460X. doi: 10.1016/j.jsv.2009.12.026.

R. Medina and M. Garrido. Improving impact-echo method by using cross-spectral density. *Journal of Sound and Vibration*, 304(3-5):769–778, July 2007. ISSN 0022460X. doi: 10.1016/j.jsv.2007.03.019.

N. S. Ottosen and M. Ristinmaa. *The mechanics of constitutive modeling*. Elsevier Science, 2005. ISBN 978-0-08-044606-6.

C. B. Park, R. D. Miller, and J. Xia. Multichannel analysis of surface waves. *Geophysics*, 64(3):800–808, May 1999. ISSN 0016-8033. doi: 10.1190/1.1444590.

J. Popovics, W. Song, J. D. Achenbach, J. H. Lee, and R. F. Andre. One-sided stress wave velocity measurement in concrete. *Journal of Engineering Mechanics*, 124(12):1346–1353, Dec. 1998. ISSN 0733-9399. doi: 10.1061/(ASCE)0733-9399(1998)124:12(1346).

J. Popovics, G. Cetrangolo, and N. Jackson. Experimental Investigation of Impact-Echo Method for Concrete Slab Thickness Measurement. *Journal of the Korean Society for Nondestructive Testing*, Vol 26(No 6):427–439, 2006.

J. Popovics, N. Ryden, and A. Gibson. New Developments in Nde Methods for Pavements. *Review of Quantitative Nondestructive Evaluation*, 27: 1320–1327, 2008. doi: 10.1063/1.2902587.

C. Prada, D. Clorennec, and D. Royer. Local vibration of an elastic plate and zero-group velocity Lamb modes. *The Journal of the Acoustical Society of America*, 124(1):203–12, July 2008. ISSN 1520-8524. doi: 10.1121/1.2918543.

L. Qixian and J. Bungey. Using compression wave ultrasonic transducers to measure the velocity of surface waves and hence determine dynamic modulus of elasticity for concrete. *Construction and building materials*, 10(4):237–242, 1996. doi: 10.1016/0950-0618(96)00003-7.

J. Roesset. Nondestructive dynamic testing of soils and pavements. *Tamkang Journal of Science and Engineering*, 1(2):61–80, 1998.

J. Roesset, D. Chang, K. Stokoe, and M. Aouad. Modulus and Thickness of the Pavement Surface Layer from SASW Tests. *Transportation Research Record*, (1260):53–63, 1990.

N. Rydén. Enhanced impact echo frequency peak by time domain summation of signals with different source receiver spacing. *Accepted for publication in the special issue on Advanced Sensing Technologies for NDE and SHM of Civil Infrastructures, Smart Structures and Systems, In press*, 2015.

N. Ryden and M. Castaings. An Adaptive Frequency Domain Finite Element Model for Surface Wave Testing of Pavements. *AIP Conference Proceedings*, 1481(2009):1481–1488, 2009. doi: 10.1063/1.3114132.

N. Ryden and C. Park. A combined multichannel impact echo and surface wave analysis scheme for non-destructive thickness and stiffness evaluation of concrete slabs. *AS NT, 2006 NDE Conference on Civil Engineering*, pages 247–253, 2006.

N. Ryden, C. B. Park, P. Ulriksen, and R. D. Miller. Multimodal Approach to Seismic Pavement Testing. *Journal of Geotechnical and Geoenvironmental Engineering*, 130(6):636–645, June 2004. ISSN 1090-0241. doi: 10.1061/(ASCE)1090-0241(2004)130:6(636).

M. Sansalone. Impact-echo: the complete story. *ACI Structural Journal*, 94 (6):777–786, 1997. ISSN 08893241. doi: 10.14359/9737.

M. Sansalone and W. Streett. *Impact-echo: Non-destructive Evaluation of Concrete and Masonry*. Bullbrier Press, 1997.

F. Schubert and B. Köhler. Ten Lectures on Impact-Echo. *Journal of Nondestructive Evaluation*, 27(1-3):5–21, July 2008. ISSN 0195-9298. doi: 10.1007/s10921-008-0036-2.

P. Shaw, J. Rasmussen, and T. Pedersen. A Practical Guide to Non Destructive Examination of Concrete. Technical report, Force Technology, Denmark, 2004. URL `http://www.nordicinnovation.org/sv/publikationer/non-destructive-testing-methods-for-integrity-determination-of-concrete-structures/`.

S. W. Shin, C. B. Yun, J. S. Popovics, and J. H. Kim. Improved Rayleigh Wave Velocity Measurement for Nondestructive Early-Age Concrete Monitoring. *Research in Nondestructive Evaluation*, 18(1):45–68, Jan. 2007. ISSN 0934-9847. doi: 10.1080/09349840601128762.

P. Shokouhi, D. Ph, J. Wolf, and H. Wiggenhauser. Detection of Delamination in Concrete Bridge Decks by Joint Amplitude and Phase Analysis of Ultrasonic Array Measurements. pages 1–11, 2014. doi: 10.1061/(ASCE)BE.1943-5592.0000513.

P. J. Shull. *Nondestructive Evaluation - Theory, Techniques, and Applications*. M. Dekker, New York, 2002. ISBN 0-8247-8872-9.

I. A. Viktorov. *Rayleigh and Lamb Waves Physical Theory and Applications*. Plenum Press, New York, 1967.

T. Wu, J. Fang, G. Liu, and M. Kuo. Determination of elastic constants of a concrete specimen using transient elastic waves. *The Journal of the Acoustical Society of America*, 98(4):2142–2148, 1995.

D. Zywicki and G. Rix. Mitigation of near-field effects for seismic surface wave velocity estimation with cylindrical beamformers. *Journal of Geotechnical and Geoenvironmental ...*, (August):970–977, 2005. doi: 10.1061/(ASCE)1090-0241(2005)131:8(970).

Part II

Appended papers

Paper I

O. Baggens and N. Ryden.
Systematic errors in Impact-Echo thickness estimation due to near field effects. NDT & E International, 69:16-27, Jan. 2015. ISSN 09638695. doi: 10.1016/j.ndteint.2014.09.003.

NDT&E International 69 (2015) 16–27

Contents lists available at ScienceDirect

NDT&E International

journal homepage: www.elsevier.com/locate/ndteint

Systematic errors in Impact-Echo thickness estimation due to near field effects

Oskar Baggens *, Nils Ryden

Division of Engineering Geology, Lund University, PO Box 118, SE-22100, Lund, Sweden

ARTICLE INFO

Article history:
Received 10 April 2014
Received in revised form
10 September 2014
Accepted 14 September 2014
Available online 22 September 2014

Keywords:
Concrete
Impact-Echo
P-wave velocity
Thickness
Near field effect

ABSTRACT

Near field effects are found to create systematic errors, within the range of about 5–15%, in thickness estimations from Impact-Echo (IE) testing. This paper studies near field effects from a point source in a combined Multichannel Analysis of Surface Waves (MASW) and Impact-Echo analysis. The near field creates deviations in the measured velocity of the P-wave and the Rayleigh-wave, which lead to an underestimated thickness. This systematic error is identified in both a numerical and a real field case. The results are also compared with the conventional Impact-Echo method.

1. Introduction

In civil engineering, efficient non-destructive quality control plays an important role in the optimization of resources for manufacturing, maintenance, and safety. For concrete construction, the thickness of plate-like structures is a parameter of particular interest [1–3]. Several techniques have emerged for determining this thickness in a non-destructive manner [4]. The Impact-Echo (IE) method is one such technique which provides a straightforward estimation of the thickness of a structure with only one accessible side.

Early studies using the IE method report thickness estimation accuracies within 3% [5]. Although recent advances show promising results for implementing non-contact scanning measurements [6], studies with more significant deviations exist [1,7,2]. In these studies the thickness is underestimated in 18 of 19 locations with a mean error of 8%. In many IE thickness testing applications, e.g. nuclear reactor containment walls or load carrying structures in bridges, a verification with a drilled core sample is often not possible. Further studies, as this paper, which can clarify and highlight difficulties and potential error sources, about IE thickness testing are therefore valuable.

The conventional IE method uses two estimated parameters: the thickness resonance frequency f_r and the P-wave velocity V_P [8]. The thickness resonance is measured from the dynamic response to a transient impact. The P-wave velocity is either measured or assumed. The thickness h is subsequently determined using the empirical relation:

$$f_r = \frac{\beta V_P}{2h} \tag{1}$$

where β is an empirical correction factor that is usually assigned the value 0.96 for concrete. In fact, the exact value of f_r corresponds to the minimum frequency of the first symmetric Lamb mode (S1) dispersion curve [9]. The group velocity is zero at this specific point (S1-ZGV) [10]. The next thickness resonance is related to the second anti-symmetric Lamb mode (A2), which is also a zero-group velocity point (A2-ZGV).

To properly evaluate plate properties such as the thickness parameter, Lamb wave theory must be used. Lamb wave theory states that a laterally infinite isotropic plate is defined by three independent parameters: the shear wave speed V_S, Poisson's ratio ν, and thickness h. Consequently, the accuracy of this type of non-destructive evaluation of plates is solely dependent on these three variables. As a result, traditional IE methods are usually complemented with some sort of surface velocity measurement to most accurately determine the thickness [11]. However, if exact values of f_r and V_P are known, an exact value of the thickness can be obtained using Eq. (1) only if a correct value of β is assumed. An alternative method of increasing accuracy is to calibrate a velocity that satisfies Eq. (1) using an exact thickness measurement from a core sample. This approach is, however, not applicable in the case of plates with one-sided access if non-destructive testing is desired.

V_P is usually estimated from the time taken by the first arriving wave to travel between two points separated by a known distance. One major source of uncertainty of the first arrival velocity is the

* Corresponding author.
E-mail address: oskar.baggens@tg.lth.se (O. Baggens).

http://dx.doi.org/10.1016/j.ndteint.2014.09.003

identification of the correct first arrival time. This uncertainty is due to the small displacement magnitude of the surface normal component of the first arriving wave. A common procedure is to identify the first value above a certain threshold, and to assume that this wave corresponds to a pure P-wave. Another approach, which may improve the identification, is to study the trend of the measured signal [12]. The velocity of the P-wave may also vary through the thickness due to a material gradient resulting from the casting of a concrete slab, if larger aggregates concentrate near the bottom of the slab [1]. Gibson showed a systematic difference between the P-wave velocity measured along the surface and through the thickness [4]. A gradient with an increasing P-wave velocity with depth has been observed by [1,13–15]. Popovics et al. proposed an additional correction factor to compensate for the slower P-wave velocity along the surface [1].

An alternative approach that eliminates difficulties in identifying the first arrival is to calculate V_P from the Rayleigh wave velocity V_R, estimated by means of spectral analysis of surface waves (SASW) [16]. This approach requires an assumed value of ν. Poisson's ratio can, for example, be determined from the ratio between the frequencies of S1-ZGV and A2-ZGV [10] or the ratio between the S1-ZGV frequency and V_R [17]. The latter approach requires a known value of the thickness.

More recent approaches use a combination of a multichannel recording and a multichannel IE analysis [18,19,7]. The specific evaluation procedures differ slightly in their approaches. However, the main concept is to introduce additional information from surface wave analysis, for example, by estimating V_R. Since at least three parameters are accessible, it is possible to incorporate Lamb wave theory. Then, all three plate parameters (V_S, ν, h) can be determined simultaneously. Compared with the traditional IE method, these types of analyses are not affected by the uncertainty of assuming a correct value of β.

A possible source contributing to the uncertainty in f_r is the presence of multiple peaks in the frequency response spectrum [20]. The use of a time frequency analysis has been suggested to enhance the identification of the correct S1-ZGV frequency [21,22]. The use of multichannel recordings is another approach to facilitate the identification of the correct S1-ZGV frequency. Summation of the traces in close vicinity to the point source can be used to make the S1-ZGV frequency more pronounced [18]. A similar approach uses a quantity described as a multicross spectral density [23].

Although several improvements to the IE method have been proposed, a remaining systematic error may result in an underestimated thickness [1,7,2]. This underestimation can occur if the P-wave velocity is underestimated or if the S1-ZGV frequency is overestimated (Eq. (1)). Of these two parameters, a velocity representative of the complete through thickness seems to be the most difficult parameter to measure. Most proposed methods are based on a P-wave and/or Rayleigh wave velocity measurement along the surface. A possible source of underestimated velocities along the surface may be due to near field effects, which in this case are due to the cylindrical spreading of waves from a point source and the interference of different wave modes [24–28]. To the authors' knowledge, the near field effect has not been previously studied in this context of combined IE and velocity measurements.

This study adopts a combined Multichannel Analysis of Surface Waves (MASW) and IE method. In conformance with the IE method, this type of analysis also assumes that the P-wave velocity can be obtained by studying the first arrival wave. The combined MASW/IE method measures the P-wave velocity (V_P), the Rayleigh wave velocity (V_R), and the S1-ZGV frequency (f_{S1-ZGV}). These three parameters are used to estimate the plate parameters V_S, ν, and h. The systematic variations of the measured parameters V_P, V_R, and f_{S1-ZGV} due to near field effects are studied for a plate without a velocity gradient with depth. These types of variations, within a few thickness distances from the source, are not specific for the studied MASW/IE method; in fact, they are present in all evaluations related to surface wave analysis and/or IE analysis. The results are therefore general for many cases. Finally, the influence of the evaluated thickness is further explored with both a synthetic and an experimental field case. The results from the MASW/IE method are also compared with the results obtained using the conventional IE method.

2. Lamb waves

Only two different wave types can exist in an isotropic infinite body, the P-wave and the S-wave [29]. In a laterally infinite plate, an additional boundary condition requires the stress traction to be equal to zero at the surfaces. Thus, it is possible for guided waves or Lamb waves to exist. Lamb waves are created from combinations of P- and S-waves that satisfy the traction-free boundary condition. An infinite number of combinations which satisfy this boundary condition exist. They are, however, governed by the same equation, the so-called Lamb wave equation:

$$\frac{\tan(\beta h/2)}{\tan(\alpha h/2)} = -\left[\frac{4\alpha\beta k^2}{(k^2-\beta^2)^2}\right]^{\pm 1} \tag{2}$$

where

$$\alpha^2 = \frac{\omega^2}{V_P^2} - k^2$$

$$\beta^2 = \frac{\omega^2}{V_S^2} - k^2$$

The Lamb wave equation is based on an assumption of plane wave propagation, and enforces that only certain combinations of wave numbers k and frequencies ω are possible. This is the origin of the dispersive nature of Lamb waves. No simple analytical solutions of the equation exist, and instead, numerical methods must be used [29]. The Lamb wave theory forms the basis for linear elastic wave propagation in plates.

The dispersive nature of Lamb waves can be illustrated in many ways. One possibility is to present dispersion curves in the frequency–phase velocity domain. Fig. 1a shows a selection of the dispersion curves (Lamb modes A0, S0, A1, and S1) for a plate with $\nu = 0.2$. The axes are normalized with the thickness h and the shear wave speed V_S. The curves are thus only dependent on ν. The curves in Fig. 1a are valid for all plates with $\nu = 0.2$.

The dispersion curves contain important information about the plate characteristics. The Rayleigh wave velocity can, for example, be determined by tracking the convergence of the phase velocity for the A0 and the S0 modes. The S1-ZGV point, which is the point of the minimum frequency of the S1-mode, is another quantity which can be determined. As mentioned before in Section 1, this point corresponds to the thickness resonance f_r used in the traditional IE method (Eq. (1)).

An expanded view of the S1-ZGV points for different values of ν is shown in Fig. 1b. The variations of the locations for the S1-ZGV points are only affected by ν. This implies that the value of fh/V_S for the S1-ZGV point is constant for a fixed value of ν, and serves as the theoretical link between the empirical β factor used in the IE method and an analytical expression as a function of ν [9,17]. The constant value of fh/V_S provides a direct way of determining the plate thickness once V_S, ν, and f_{S1-ZGV} are known.

The constant value of fh/V_S also reveals how the estimated thickness is affected by uncertainties in the quantities V_S, ν, or f_{S1-ZGV} (Fig. 1b). An overestimation of f_{S1-ZGV} yields an

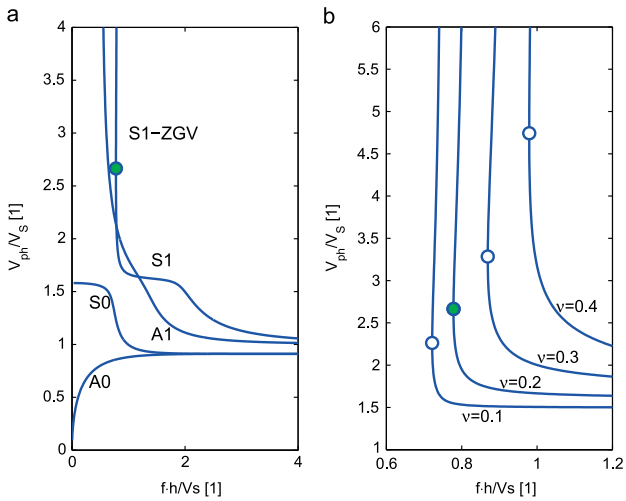

Fig. 1. (a) Lamb wave dispersion curves (A0, S0, A1, and S1 modes). (b) Expanded view around S1-ZGV points (S1 mode).

underestimated thickness, whereas an overestimation of V_S yields an overestimated thickness, assuming that the other two constants are exact. Finally, an overestimation of ν results in an overestimated thickness (Fig. 1b).

In practice, the plate parameters V_S, ν, and h are in most cases not directly accessible. Therefore, they must be determined indirectly using other parameters. One possibility is to measure V_P, V_R, and f_{S1-ZGV}, for example, by means of a combined MASW/IE method [18]. These three quantities provide the necessary information to determine V_S, ν, and h, and this approach was adopted in this study. The accuracy of the thickness estimation, which is of particular interest, is therefore dependent on the accuracy of the indirect parameters V_P, V_R, and f_{S1-ZGV}.

3. Numerical modeling

The presented theory in Section 2 assumes plane wave propagation, which at several wavelength's distance is a good approximation even for waves generated by a point source. As the radial distance of the studied waves decreases, this assumption becomes less valid, and near field effects are present. Furthermore, close to the source several different wave modes (e.g. P-waves, S-waves, Rayleigh waves) interfere with each other. A suitable approach for studying these two factors (i.e. near field effects) and the transition to the far field is to use a numerical model. A synthetic model, by means of Finite Elements (FE), was created in order to investigate the accuracy of the V_P, V_R, and f_{S1-ZGV} estimates determined by a combined MASW/IE technique. The model was created using commercial finite element software, Comsol Multiphysics [30]. A 2D axial symmetric plate was defined using a linear elastic material with Young's modulus of 36.1 MPa and a density of 2197 kg/m^3. The model was calculated using Poisson's ratios of 0.1, 0.2, 0.3, and 0.4, thus, covering a wide range of possible materials.

The thickness was set to 0.261 m and the length of the plate was 25 times longer than the thickness (Fig. 2). A short line load at the top surface was applied to simulate a point source. The load started at the symmetry axis and had a radius of 0.0025 m.

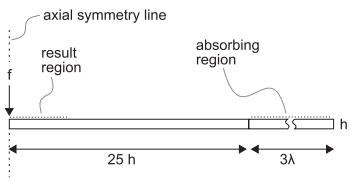

Fig. 2. FE-model sketch.

The plate was studied in the frequency domain, solving for the complex steady state response. A triangular element mesh with quadratic shape functions was used. A fine mesh with a minimum element length of 0.0025 m was used around the source location. In the rest of the model the element mesh was adjusted to have at least 10 elements per wavelength of the A0 mode. The mesh was thus adjusted for the solved frequencies using a coarse mesh for the low frequencies and a finer mesh for the high frequencies [31].

A silent boundary was created by a gradually increasing damping ratio in the absorbing region [32]. This region was added as an extension to the plate (Fig. 2). The length of the absorbing region was adjusted for the solved frequency with a length of 3 times the wavelength of the P-wave. The defined mesh and absorbing parameters were determined by a parametric convergence study of the theoretical Rayleigh wave velocity and S1-ZGV frequency.

In order to simulate the Impact-Echo and surface wave test, three synthetic force pulses were defined. The pulses were based on the Gaussian mono-pulse with different frequency contents (Fig. 3). The Gaussian mono-pulse was chosen to avoid energy at 0 Hz, as this energy can be difficult to handle in frequency domain simulations of a free plate. The pulses can be characterized as a low-frequency, mid-frequency, and high-frequency pulse with regard to the S1-ZGV frequencies (7–9 kHz) of the simulated plates.

The frequency domain responses along the upper surfaces of the plates from the pulses were calculated using the result from

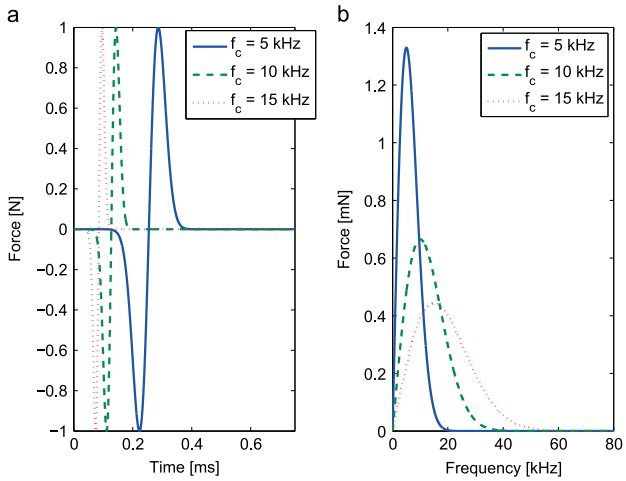

Fig. 3. Force pulses: (a) time domain, (b) frequency domain.

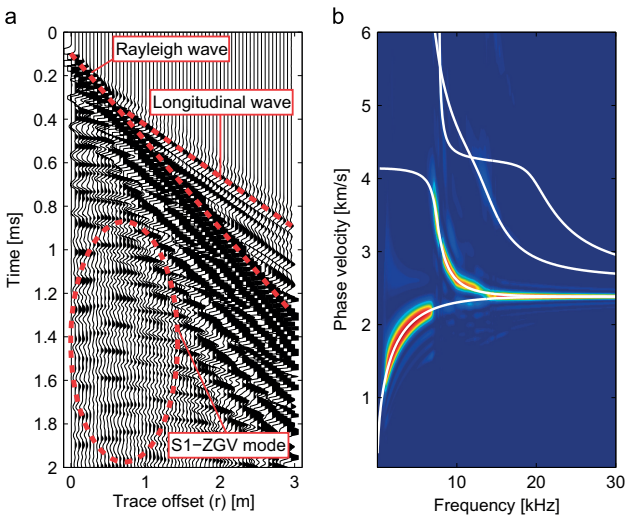

Fig. 4. Dataset: (a) time domain, (b) phase velocity–frequency domain.

the steady state analysis (Fig. 2). Subsequently, an inverse Fourier transform was performed to generate the response for the pulses in the time domain [32]. This concept was used to create synthetic multichannel datasets (Fig. 4a). The datasets were transformed into the phase velocity–frequency domain (Fig. 4b) [33]. It could be seen that the theoretical Lamb wave curves correlated well with the synthetic datasets. A detailed analysis of the difference between the simulated and theoretical values will be studied in the subsequent Results section.

4. Results

Estimates of the first arrival P-wave velocity (V_P), the Rayleigh wave velocity (V_R), and the S1-ZGV frequency (f_{S1-ZGV}) have been studied as a function of distance from the source in order to quantify the influence of the near field. In all the presented result plots the distance from the source has been expressed as radius divided by thickness (r/h). This scale is used to emphasize that results are roughly applicable to any plate thickness although an

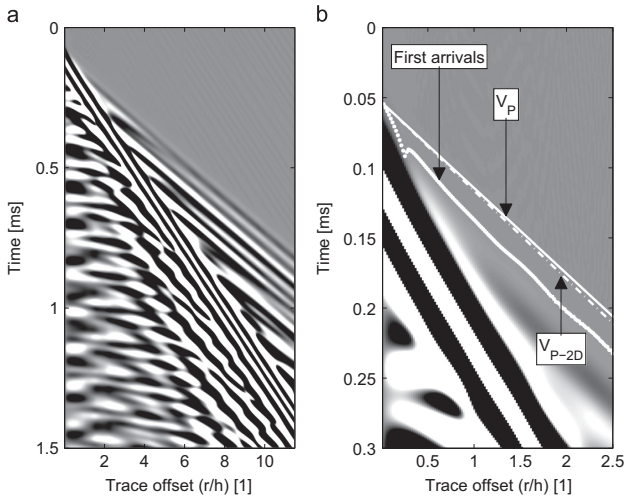

Fig. 5. Dataset $\nu=0.2$, $f_c=10$ kHz: (a) time domain, (b) expanded view, first arrivals.

exact normalization in both time (frequency) and space (wavelength) is not possible.

4.1. P-wave velocity

The variation of the first arrival P-wave velocity as a function of distance was studied for plate models with different values of ν. The models were studied in the time domain using the mid-frequency pulse (see Fig. 3). Fig. 5a shows the surface normal acceleration response to the mid-frequency pulse for the plate with $\nu=0.2$. The surface normal acceleration response was subsequently used to determine the first arrival P-wave.

Signals were gained in order to enhance the picture of the wave field and the first arrivals (Fig. 5b). In this type of commonly used seismic plot, the first arrival velocity close to the impact source appears to be close to the Rayleigh wave velocity. At a distance of about 1/4 of the thickness, there is a jump to a faster first arrival velocity which is closer to the P-wave velocity. The hidden first arrival of the P-wave is a consequence of the huge difference in amplitude of the Rayleigh wave and the P-wave (interference of modes).

First arrivals were picked for each trace at time points corresponding to the first absolute values above a threshold limit (Fig. 5b). The threshold limit was set at 10^{-4} of the maximum absolute value of the amplitude in each individual trace. Consequently, the threshold limit was reduced with an increasing radial distance. Fig. 5b also shows the theoretical first arrival P-wave velocity (V_P) along with the slightly slower quasi-P-wave velocity in plates (V_{P-2D}), marked with dotted lines. V_{P-2D} corresponds to the low frequency asymptotic value of the S0 Lamb mode in plates (Fig. 1a) and is the expected low frequency P-wave velocity in a plate [29]. The theoretical first arrivals were adjusted to intersect with the first arrival of the first trace.

The P-wave velocity was calculated by adjusting a slope to the first arrivals using linear regression. This evaluation was repeated while adding new traces to the array, and thus the length of the array was gradually extended. In all evaluations, the first trace was located at a fixed offset of 0.005 m from the impact center. This type of evaluation corresponds to a typical combined MASW/IE analysis.

In order to simulate the procedure used in the IE standard, the first arrival P-wave velocity was also calculated using two traces only. The first trace was selected at an offset of 0.005 from the impact center, and the second trace was selected at a distance of 0.3 from the first trace. The time difference of the first arrivals and the known distance of 0.3 m between the traces were used to yield the first arrival P-wave velocity. This calculation was repeated for different offset locations of the two traces, while maintaining a fixed internal distance between the traces of 0.3 m. This type of evaluation corresponds to the conventional Impact-Echo procedure when the first transducer is located at an offset of 0.15 m from the impact center [11].

The results from the MASW/IE and the IE type of analysis of the first arrivals are shown in Fig. 6a and b, respectively. The extracted velocities have been normalized with the theoretical P-wave velocity for each Poisson's ratio. In both types of analysis the initial normalized first arrival velocity close to the impact source is lower than the theoretical values. At a greater distance from the source, the normalized first arrival velocity gradually approaches the theoretical value. It can also be noticed that the sign of acceleration response (i.e., the direction) of the first arrivals is not constant and causes a discontinuity in the curve located at an offset of about 1/4 thickness. This shift of sign explains the momentarily high velocities of the IE type of analysis (Fig. 6b).

For Poisson's ratios 0.1 and 0.4, there are also other phase shifts at greater distances from the source. These phase shifts are caused by Lamb wave dispersion and generate extreme velocities in the IE analysis. Therefore, the first arrival P-wave velocity was only tracked until such an event occurred (Fig. 6b). The MASW/IE type of analysis is not affected in the same way, and it presents a more stable trend since it is based on an evaluation using multiple traces. It is also observed that the results for both evaluation methods are dependent on ν.

The above studied methods for determining the first arrival P-wave velocity are time domain evaluations, as are normally performed in practice. This type of analysis does not account for the dispersion which is typical for Lamb waves (Fig. 4b). Therefore, the dependency of frequency needed to be explored further.

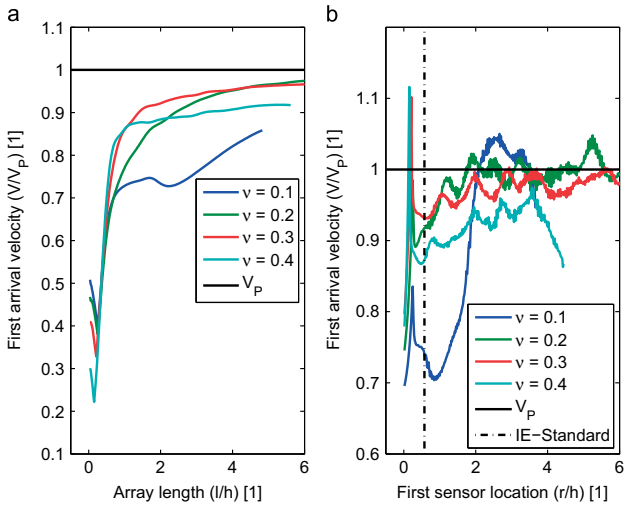

Fig. 6. First arrival velocity: (a) MASW/IE, (b) IE.

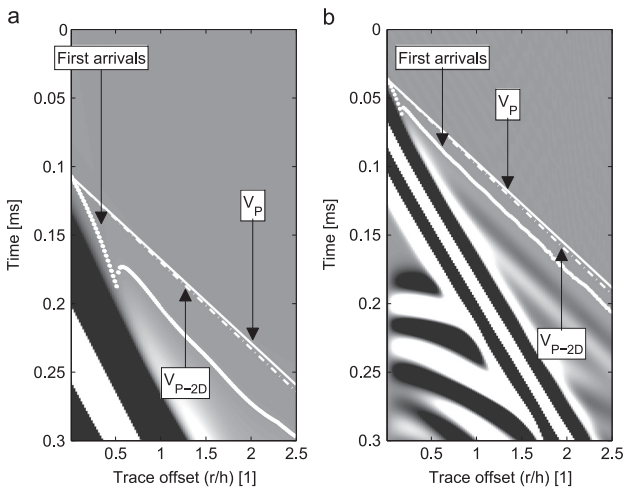

Fig. 7. Dataset, first arrivals: (a) $\nu=0.2$, $f_c=5$ kHz, (b) $\nu=0.2$, $f_c=15$ kHz.

The plate model with $\nu=0.2$ was chosen for a study using different pulses. The variation of the first arrival P-wave velocity as a function of distance was studied for the low, mid-, and high-frequency pulses. The surface normal acceleration responses of the low- and high-frequency pulses are shown in Fig. 7a and b, respectively.

It can be seen that the response of the low-frequency pulse (Fig. 7a) creates a larger zone with a slower first arrival velocity compared to that of the high-frequency pulse (Fig. 7b). This is consistent with the condition that a low-frequency pulse generates a response with a longer wavelength. The same type of evaluations for the first arrival P-wave velocity based on the MASW/IE and IE methods was performed for the different pulses. The results are shown in Fig. 8a and b. It can be noticed that variations in the estimated first arrival P-wave velocities are also dependent on the frequency content of the exciting pulses.

4.2. Rayleigh wave velocity, S1-ZGV frequency

The variation in V_R was studied for the plates with different values of ν. The mid-frequency pulse was used to create the

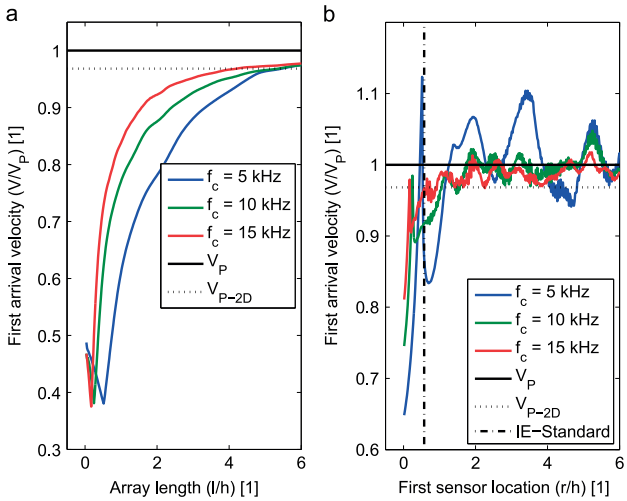

Fig. 8. First arrival velocity: (a) MASW/IE, (b) IE.

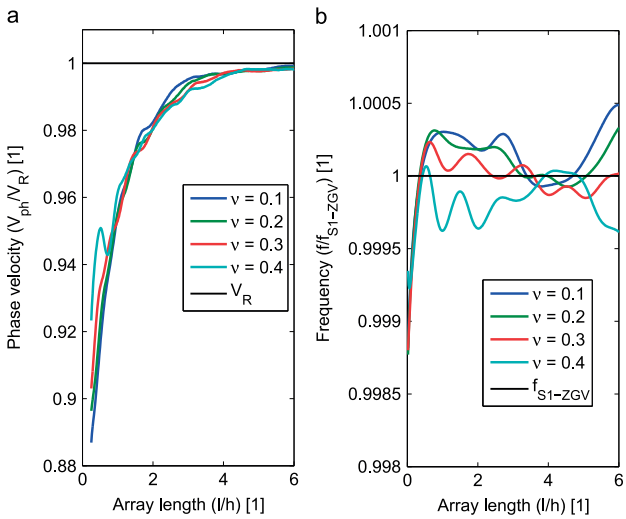

Fig. 9. (a) Rayleigh-wave velocity. (b) S1-ZGV frequency.

datasets. V_R was estimated by tracking the convergence of the A0 and S0 modes of the datasets in the frequency–phase velocity domain. This evaluation was made for different array lengths. The array was extended by adding new traces as with the study of the first arrival P-wave velocity. The extracted velocity is shown in Fig. 9a. It can be observed that V_R is underestimated close to the source, i.e. when the array in the combined MASW/IE method is short. Thereafter, the estimated velocity gradually increases and converges with the theoretical velocity when the array lengthens. The estimated velocity is dependent on ν. However, the main behavior is generally the same for all values of ν. The observed phenomena are in agreement with the results obtained by [26,28] for V_R in a half space. Roesset [26] showed analytically how the phase velocity for the response at the surface increases with the distance from the source in the case of a homogeneous half-space. This slower phase velocity close to the source is related to the variation in the interference between the bulk wave modes. For the studied case shown in Fig. 9a, the near-field effect is likely to

be even more complicated, since the geometry is a plate instead of a half-space. Furthermore, the use of an array as well as the frequency content of the impulse may also add additional complexity to the problem. Therefore, the result shown in Fig. 9a should not be interpreted exactly quantitatively but rather as a general trend partly explaining the observed underestimated thickness.

The S1-ZGV frequency was estimated using an offset summation technique [18]. This technique was used in the combined MASW/IE analysis to enhance the S1-ZGV resonance frequency peak [7]. The evaluation was made for different array lengths in the same manner as with the evaluation of V_R. The results from the S1-ZGV frequency estimations are shown in Fig. 9b. These estimations do not provide a completely constant value; instead, they oscillate slightly. These minor variations were assumed to be associated with uncertainties inherited from the nature of numerical modelling and evaluations. However, in comparison with the estimations of V_P and V_R, the estimations of f_{S1-ZGV} can be considered as accurate.

4.3. Thickness

The above demonstrated variations in the estimations of V_P and V_R indicate that a systematic error is present using the MASW/IE or the IE method. Thus, a systematic error is also present if the thickness is calculated from the estimations of V_P and V_R.

An estimate of the thickness as a function of distance was therefore calculated by combining the results in Figs. 6 and 9 from the mid-frequency source (f_c=10 kHz). These calculations were made using both the MASW/IE and IE techniques. In the MASW/IE analysis, ν was calculated from ratio of the first arrival P-wave velocity and the Rayleigh wave velocity. In this evaluation the first arrival P-wave velocity was assumed to correspond to the theoretical velocity of V_P. Thereafter, the thickness was calculated from the constant value of the quantity fh/V_S, as described in Section 2. The IE analysis used values of the first arrival P-wave velocity from Fig. 6b and a fixed value of the S1-ZGV frequency. This fixed value was extracted from the frequency spectrum of one single trace at a distance of 0.05 m from the source. The thickness was subsequently estimated using Eq. (1) with β=0.96 to mimic a real case evaluation where ν in general is not known beforehand. The estimated thicknesses by the MASW/IE and the IE method are shown in Fig. 10a and b, respectively.

For the MASW/IE analysis, ν was generally underestimated due to the underestimated ratio between the first arrival P-wave velocity and the Rayleigh wave velocity. Therefore, in the case of the model with a ν=0.1, it was not possible to estimate the thickness since the Lamb wave equation only was solved for values of ν from 0.10 to 0.45 (with increments of 0.01). This fixed increment of 0.01 explains the discontinuities in the curves in Fig. 10a. It can be observed that the MASW/IE type of method underestimates the thickness (Fig. 10a). As the estimates of V_P and V_R become more accurate, the estimated thickness subsequently becomes more accurate. Similar results were obtained from datasets with source frequencies f_c=5 kHz and f_c=15 kHz, although they are not plotted here. It should also be noticed that the alternative interpretation of the first arrival P-wave velocity as V_{P-2D} does not improve the results.

The estimated thickness from the IE method shows a more fluctuating result with a higher relative error compared to the MASW/IE analysis (Fig. 10b). The variation in the thickness (Fig. 10b) follows the variation of the estimated value of V_P (Fig. 6b), since the values for β and f_r were given a constant value when Eq. (1) was evaluated. It can be observed that the IE method for the case of this quite unrealistic value of ν=0.4 overestimates the thickness. This is due to the fixed value of β=0.96. A more suitable value would have been around 0.80 [9,17]. However, with real case data, the value of ν typically is not known beforehand. The analysis was therefore made with a fixed value of 0.96 for the β factor.

In the standard IE velocity measurement of the first arrival P-wave the estimated thickness is actually quite close to the true value (within 4%) after $r/h > 2$. With this set-up the problematic near field effect for a homogeneous plate is effectively minimized.

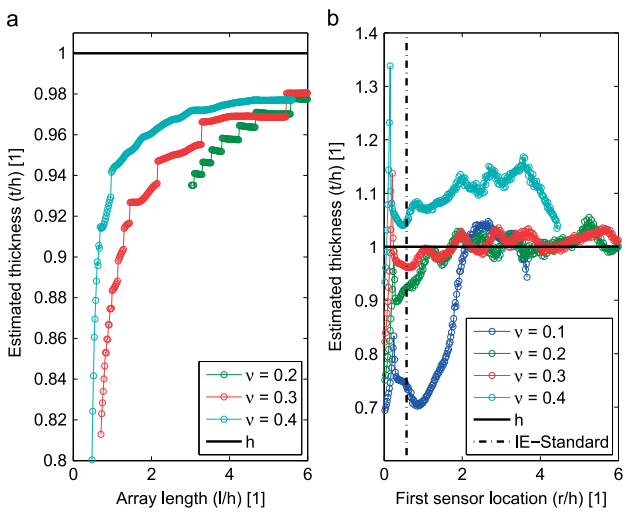

Fig. 10. Estimated thickness: (a) MASW/IE, (b) IE.

For the studied plate and source frequency this result is valid for all Poisson's ratios, except the quite unrealistic value of $\nu = 0.4$ for concrete.

5. Field case

The systematic error presented in Fig. 10 was further explored by studying a real field case. The aim of this field study was to investigate to which extent the near field effects could be observed in a real practical case. Field data was obtained from a Portland concrete cement plate cast on a granular base at The Advanced Transportation Research and Engineering Laboratory (ATREL), University of Illinois at Urbana-Champaign (UIUC). This plate is at the same location as location 5 in [7]. In this point the thickness was underestimated with all tested seismic techniques (4–13%).

Time-synchronized multichannel data were obtained using one accelerometer and a hammer with a trigger connected to a DAQ computer [34]. The accelerometer measured the surface normal component of the acceleration response. Data were collected over a distance of 1 m with an interval distance of 0.02 m between each hammer impact. The data could therefore be used for a MASW/IE and an IE analysis using the same evaluation techniques previously described. A core sample was also extracted from the center of the 1 m long MASW/IE array. The thickness was measured to 0.337 m [7].

A plot of the data in time domain and frequency–phase velocity domain can be seen in Fig. 11a and b, respectively. The locations of the first arrivals are marked with black dots in Fig. 11a. The first arrivals were identified at time points corresponding to the first absolute value exceeding a threshold limit. This threshold limit was set at 2.5×10^{-3} of the maximum absolute value in each individual trace. As in the synthetic case, the threshold limit was reduced with an increasing radial distance.

The indirect plate parameters V_P, V_R, and f_{S1-ZGV} were estimated in the same way as with the synthetic dataset. Estimations of the parameters were repeated using a different number of signals from the dataset, i.e., for different lengths of the measuring array. Thus, it was possible to create plots, similar to those previously presented, for the variation of the parameters with respect to the array length.

5.1. P-wave and Rayleigh wave velocity, S1-ZGV frequency

The variation of the first arrival P-wave velocity for the MASW/IE analysis can be seen in Fig. 12a. Fig. 12b shows the variation of the first arrival P-wave velocity using the IE type of measurement.

It can be observed that the first arrival P-wave velocity increases with the array length or the location of the sensors. This is the same general trend as with the synthetic case. The observed low resolution in Fig. 12b is a consequence of the low sample rate in the field data ($dt = 5\ \mu s$) compared to the synthetic data case ($dt = 0.1\ \mu s$). Ideally, a higher sample rate with lower value than $dt = 5\ \mu s$ should therefore be used.

It should be noted that a refracted P-wave can cause a similarly increasing velocity with distance due to an increasing stiffness within the concrete layer. In the analyzed test location, a velocity gradient ($V_P = 4450$ m/s, 4765 m/s, 4828 m/s, from top to bottom) was actually observed by ultrasonic pulse velocity measurements of different sections of the extracted core sample. Assuming a top lower velocity layer with a thickness 0.05 m, a two-layer refraction model analysis can be made. From this, it is possible to estimate the radial distance for an appearance of a refracted P-wave [35]. It was found that a higher velocity from refraction could be predicted at a distance starting from about 1.5 thicknesses. Thus, it can be concluded that the material gradient cannot be the only explanation of the slower velocity close to the source in Fig. 12. Therefore, the consequence of the gradient in this case may act as an additional contribution to an increasing velocity with distance.

The estimations of the Rayleigh wave velocity and the S1-ZGV frequency are shown in Fig. 13a and b, respectively.

It can be seen in Fig. 13a that the Rayleigh wave velocity takes a lower value close to the source. Regarding the S1-ZGV frequency in Fig. 13b, a minor variation of the frequency is found. It was assumed that the S1-ZGV frequency also in this case could be

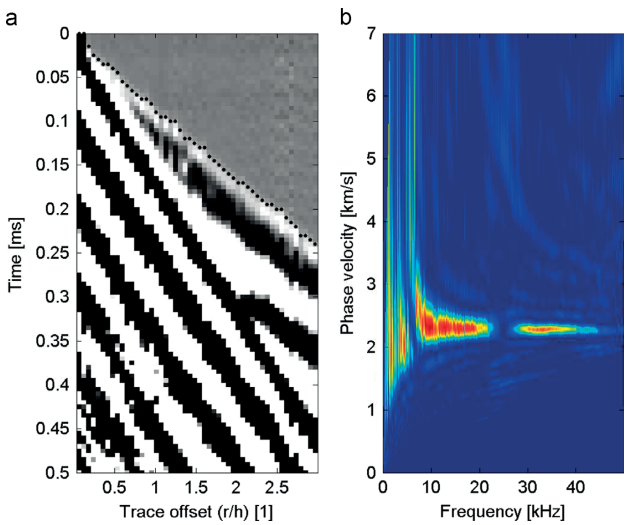

Fig. 11. Field data: (a) time domain, (b) phase velocity–frequency domain.

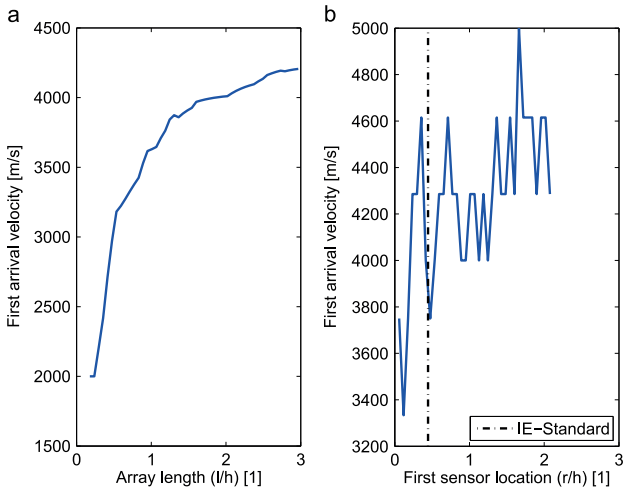

Fig. 12. First arrival velocity: (a) MASW/IE, (b) IE.

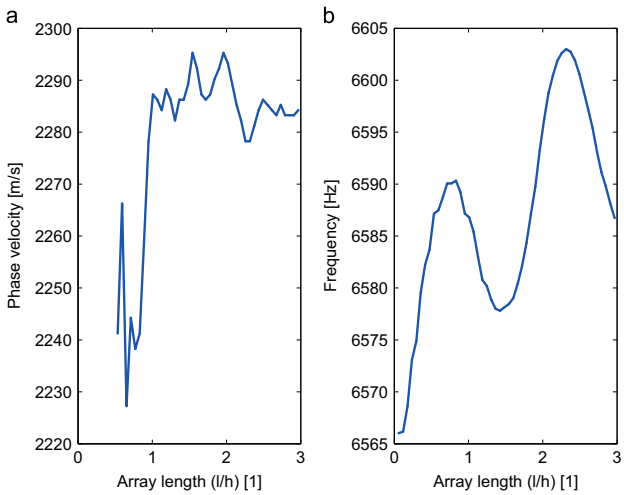

Fig. 13. (a) Rayleigh-wave velocity. (b) S1-ZGV frequency.

estimated with good accuracy. These observations for the Rayleigh wave velocity and S1-ZGV frequency are in agreement with the results obtained from the synthetic case.

Although the variations of the estimated parameters in Figs. 12 and 13 are not identical to the results from the synthetic dataset, it is possible to identify a common general behavior. It can also be observed that the estimated first arrival P-wave velocity shows the largest relative variation of the estimated quantities. The Rayleigh wave velocity shows the second largest relative variation, whereas the estimation of the S1-ZGV frequency only shows a minor relative variation. This result of the relative variation in the estimated parameters is in agreement with the result from the synthetic case.

5.2. Thickness

The estimations of V_P, V_R, and f_{S1-ZGV} were then subsequently used to calculate the variation in the corresponding estimated thickness. This calculation was made for the MASW/IE and IE types of methods, and followed the same procedure as for the synthetic case. The variation of the estimated thickness for the MASW/IE and IE types of methods can be seen in Fig. 14a and b, respectively.

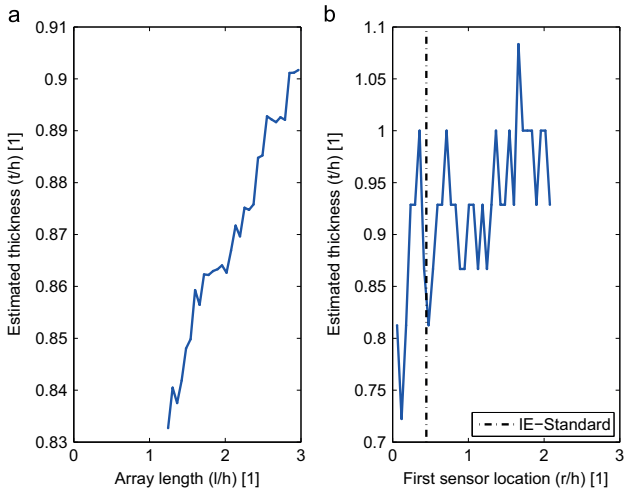

Fig. 14. Estimated thickness: (a) MASW/IE, (b) IE.

Fig. 14a shows that the MASW/IE analysis underestimates the thickness, especially when the array length is short. For the IE method in Fig. 14b, the thickness is underestimated in most cases. The IE method also shows a more fluctuating result due to the variation of V_P. It should be noted that part of this fluctuation originates from the relatively low sample rate. The general trend in Fig. 14 agrees qualitatively with the synthetic data presented in Fig. 10 within a distance of 3 thicknesses. It should be noted that longer array lengths are often unsuitable in practice and not desired since local plate properties are then smeared out. The observed larger underestimation in the field case, compared with the synthetic case, could be caused by the velocity gradient within the layer [1].

6. Conclusions

Numerical results show that near field effects can cause a systematic error in the estimation of thickness using a MASW/IE or a conventional IE method. The major source of error in the thickness estimations is related to the interpretation of the first arrival as a pure P-wave velocity. Detailed numerical analyses close to the point source reveal strong interference between the P-wave and the Rayleigh wave in the near field. This results in a zone where the first arrival velocity cannot be directly linked to the theoretical P-wave velocity. Furthermore, the size of this zone close to the point source is dependent on the plate properties and the source frequency content. This near field effect leads to an underestimated P-wave velocity from the picked first arrivals. These results further verify the inherently difficult and questionable task of estimating the P-wave velocity from first arrivals of dispersive Lamb waves.

The Rayleigh wave is also affected by the near field effect. Close to the point source, a lower value than the theoretical Rayleigh wave velocity is observed.

The S1-ZGV frequency is in general estimated with good accuracy.

The combined errors due to the near field effects create a systematic error which underestimates the thickness. This predicted systematic error of the estimated thickness from the MASW/IE and IE methods is found to be about 5–15% depending on Poisson's ratio, measurement set-up and source pulse. These findings are important for future improvements of non-destructive methods, such as the MASW/IE and IE methods.

Acknowledgments

Professor John S. Popovics is acknowledged for providing the experimental test site at The Advanced Transportation Research and Engineering Laboratory (ATREL), University of Illinois at Urbana-Champaign (UIUC) and for providing additional reference data of core samples. Professor Michael Lowe is acknowledged for valuable comments and discussions during the course of this study. The Development Fund of the Swedish Construction Industry (SBUF, No. 12534) and The Swedish Radiation Safety Authority (SSM, No. SSM2012-890) are acknowledged for financing the study.

References

[1] Popovics J, Cetrangolo G, Jackson N. Experimental investigation of impact-echo method for concrete slab thickness measurement. J Korean Soc Nondestruct Test 2006;26(6):427–39 URL ⟨http://www.dbpia.co.kr/Journal/ArticleDetail/3207698⟩.
[2] Maser KR. Non-destructive measurement of pavement layer thickness. Technical report. California Department of Transportation; 2003.
[3] Deacon JA, Monismith CL, Harvey JT. Pay factors for asphalt-concrete construction: effect of construction quality on agency costs. Technical report. Pavement Research Center, Institute of Transportation Studies, University of California, Berkeley; 1997.
[4] Gibson A. Advances in nondestructive testing of concrete pavements [Ph.d. thesis]. University of Illinois; 2004.
[5] Sansalone M, Streett W. Impact-echo: non-destructive evaluation of concrete and masonry. Jersey Shore: Bullbrier Press; 1997.
[6] Zhu J, Popovics JS. Imaging concrete structures using air-coupled impact-echo. J Eng Mech 2007;133(6):628–40. http://dx.doi.org/10.1061/(ASCE)0733-9399(2007)133:6(628) URL ⟨http://www.scopus.com/inward/record.url?eid=2-s2.0-34249020731&partnerID=tZOtx3y1⟩.
[7] Popovics J, Ryden N, Gibson A. New developments in NDE methods for pavements. Rev Quant Nondestruct Eval 2008;27:1320–7 URL ⟨http://scitation.aip.org/content/aip/proceeding/aipcp/10.1063/1.2902587⟩.

[8] Sansalone M. Impact-echo: the complete story. ACI Struct J 1997;94(6):777–86. http://dx.doi.org/10.14359/9737 URL ⟨http://www.concrete.org/Publications/ACIMaterialsJournal/ACIJournalSearch.aspx?m=details&ID=9737⟩.

[9] Gibson A, Popovics J. Lamb wave basis for impact-echo method analysis. J Eng Mech 2005;1–6. doi: http://dx.doi.org/10.1061/(ASCE)0733-9399(2005)131:4(438). URL ⟨http://ascelibrary.org/doi/abs/10.1061/(ASCE)0733-9399(2005)131:4(438)⟩.

[10] Clorennec D, Prada C, Royer D. Local and noncontact measurements of bulk acoustic wave velocities in thin isotropic plates and shells using zero group velocity Lamb modes. J Appl Phys 2007;101(3):034908. http://dx.doi.org/10.1063/1.2434824 URL ⟨http://link.aip.org/link/JAPIAU/v101/i3/p034908/s1&Agg=doi⟩.

[11] ASTM C 1383, Standard test method for measuring the P-wave speed and the thickness of concrete plates using the impact-echo method, annual book of American society for testing and materials (ASTM) standards.

[12] Popovics J, Song W, Achenbach JD, Lee JH, Andre RF. One-sided stress wave velocity measurement in concrete. J Eng Mech 1998;124(12):1346–53. http://dx.doi.org/10.1061/(ASCE)0733-9399(1998)124:12(1346) URL ⟨http://www.scopus.com/inward/record.url?eid=2-s2.0-0032455153&partnerID=tZOtx3y1http://ascelibrary.org/doi/abs/10.1061/(ASCE)0733-9399(1998)124:12(1346)⟩.

[13] Hu M, Lin Y, Cheng C. Method for determining internal P-wave speed and thickness of concrete plates. ACI Mater J 2006;103(5):327–35. http://dx.doi.org/10.14359/18154 URL ⟨http://www.concrete.org/Publications/ACIMaterialsJournal/ACIJournalSearch.aspx?m=details&ID=18154⟩.

[14] Qixian L, Bungey J. Using compression wave ultrasonic transducers to measure the velocity of surface waves and hence determine dynamic modulus of elasticity for concrete. Constr Build Mater 1996;10(4):237–42. http://dx.doi.org/10.1016/0950-0618(96)00003-7 URL ⟨http://www.sciencedirect.com/science/article/pii/0950061896000037⟩.

[15] Boyd A, Ferraro C. Effect of curing and deterioration on stress wave velocities in concrete. J Mater Civil Eng 2005;(April):153–158. doi:http://dx.doi.org/10.1061/(ASCE)0899-1561(2005)17:2(153). URL ⟨http://ascelibrary.org/doi/abs/10.1061/(ASCE)0899-1561(2005)17:2(153)⟩.

[16] Kim D, Seo W, Lee K. IE-SASW method for nondestructive evaluation of concrete structure. NDT & E Int 2006;39(2):143–54. http://dx.doi.org/10.1016/j.ndteint.2005.06.009 URL ⟨http://linkinghub.elsevier.com/retrieve/pii/S0963869505001003⟩.

[17] Medina R, Bayón A. Elastic constants of a plate from impact-echo resonance and Rayleigh wave velocity. J Sound Vib 2010;329(11):2114–26. http://dx.doi.org/10.1016/j.jsv.2009.12.026 URL ⟨http://linkinghub.elsevier.com/retrieve/pii/S0022460X0901027X⟩.

[18] Ryden N, Park C. A combined multichannel impact echo and surface wave analysis scheme for non-destructive thickness and stiffness evaluation of concrete slabs. In: AS NT, 2006 NDE conference on civil engineering; 2006. p. 247–53. URL ⟨http://scholar.google.com/scholar?hl=en&btnG=Search&q=intitle:A+Combined+Multichannel+Impact+Echo+and+Surface+Wave+Analysis+Scheme+for+Non-destructive+Thickness+and+Stiffness+Evaluation+of+Concrete+Slabs#0⟩.

[19] Barnes CL, Trottier J-F. Hybrid analysis of surface wavefield data from Portland cement and asphalt concrete plates. NDT & E Int 2009;42(2):106–12. http://dx.doi.org/10.1016/j.ndteint.2008.10.003 URL ⟨http://linkinghub.elsevier.com/retrieve/pii/S0963869508001217⟩.

[20] Schubert F, Wiggenhauser H, Lausch R. On the accuracy of thickness measurements in impact-echo testing of finite concrete specimens—numerical and experimental results. Ultrasonics 2004;42(1–9):897–901. http://dx.doi.org/10.1016/j.ultras.2004.01.076 URL ⟨http://www.ncbi.nlm.nih.gov/pubmed/15047403⟩.

[21] Abraham O, Leonard C, Cote P, Piwakowski B. Time frequency analysis of impact-echo signals: numerical modeling and experimental validation. ACI Mater J 2000;97:645–57. http://dx.doi.org/10.14359/9978 URL ⟨http://www.concrete.org/Publications/ACIMaterialsJournal/ACIJournalSearch.aspx?m=details&ID=9978⟩.

[22] Algernon D, Wiggenhauser H. Impact echo data analysis based on Hilbert–Huang transform. Transp Res Rec 2007;2028(1):146–53. http://dx.doi.org/10.3141/2028-16 URL ⟨http://www.scopus.com/inward/record.url?eid=2-s2.0-41549088922&partnerID=tZOtx3y1⟩.

[23] Medina R, Garrido M. Improving impact-echo method by using cross-spectral density. J Sound Vib 2007;304(3–5):769–78. http://dx.doi.org/10.1016/j.jsv.2007.03.019 URL ⟨http://linkinghub.elsevier.com/retrieve/pii/S0022460X07001824⟩.

[24] Zywicki D, Rix G. Mitigation of near-field effects for seismic surface wave velocity estimation with cylindrical beamformers. J Geotech Geoenviron Eng 2005;(August):970–977. doi:http://dx.doi.org/10.1061/(ASCE)1090-0241(2005)131:8(970). URL ⟨http://ascelibrary.org/doi/abs/10.1061/(ASCE)1090-0241(2005)131:8(970)⟩.

[25] Roesset J, Chang D, Stokoe K, Aouad M. Modulus and Thickness of the Pavement Surface Layer from SASW Tests. Transp Res Rec 1990;1260:53–63.

[26] Roesset J. Nondestructive dynamic testing of soils and pavements. Tamkang J Sci Eng 1998;1(2):61–80 URL ⟨http://www.researchgate.net/publication/237809455_Nondestructive_Dynamic_Testing_of_Soils_and_Pavements/file/72e7e52a9e73922ae7.pdf⟩.

[27] Ditri J, Pilarski A. Generation of guided waves in a plate by axisymmetric normal surface loading. In: Review of progress in quantitative nondestructive evaluation, vol. 13. URL ⟨http://books.google.com/books?hl=en&lr=&id=RWulSz94GPAC&oi=fnd&pg=PA133&dq=Generation+of+Guided+waves+in+a+plate+by+axisymnetric+normal+surface+loading&ots=CsnCME1_0P&sig=_5TG40-ePmiFOh187QJ4o5t5WBw⟩.

[28] Bodet L, Abraham O, Clorennec D. Near-offset effects on Rayleigh-wave dispersion measurements: physical modeling. J Appl Geophys 2009;68(1):95–103. http://dx.doi.org/10.1016/j.jappgeo.2009.02.012 URL ⟨http://www.scopus.com/inward/record.url?eid=2-s2.0-67349207134&partnerID=tZOtx3y1⟩.

[29] Achenbach JD. Wave propagation in elastic solids. Amsterdam, London: North-Holland Publishing Company; 1973.

[30] Comsol Inc, Comsol Multiphysics, 2014. URL ⟨http://www.comsol.com⟩.

[31] Ryden N, Castaings M, Thompson DO, Chimenti DE. An adaptive frequency domain finite element model for surface wave testing of pavements. AIP Conf Proc 2009;1096:1481–8. doi:http://dx.doi.org/10.1063/1.3114132. URL ⟨http://link.aip.org/link/APCPCS/v1096/i1/p1481/s1&Agg=doi⟩.

[32] Castaings M, Bacon C, Hosten B, Predoi MV. Finite element predictions for the dynamic response of thermo-viscoelastic material structures. J Acoust Soc Am 2004;115(3):1125. http://dx.doi.org/10.1121/1.1639332 URL ⟨http://www.scopus.com/inward/record.url?eid=2-s2.0-1542376817&partnerID=tZOtx3y1⟩.

[33] Park CB, Miller RD, Xia J. Multichannel analysis of surface waves. Geophysics 1999;64(3):800–8. http://dx.doi.org/10.1190/1.1444590 URL ⟨http://library.seg.org/doi/abs/10.1190/1.1444590⟩.

[34] Ryden N, Park CB, Ulriksen P, Miller RD. Multimodal approach to seismic pavement testing. J Geotech Geoenviron Eng 2004;130(6):636–45. http://dx.doi.org/10.1061/(ASCE)1090-0241(2004)130:6(636) URL ⟨http://www.scopus.com/inward/record.url?eid=2-s2.0-2942608989&partnerID=tZOtx3y1⟩.

[35] Sheriff RE. Encyclopedic dictionary of exploration geophysics, geophysical references series, vol 1. Society of Exploration, Tulsa; 1991.

Paper II

O. Baggens and N. Ryden.
Poisson's ratio from polarization of zero-group velocity Lamb mode. Submitted for publication (Journal of the Acoustical Society of America). 2015.

Poisson's ratio from polarization of zero-group velocity Lamb mode

Oskar Baggens, Nils Ryden
Div. of Engineering Geology, Lund University, Sweden
PO Box 118, SE-22100, Lund, Sweden
oskar.baggens@tg.lth.se, nils.ryden@tg.lth.se

Abstract: Poisson's ratio is estimated from the polarization of the first symmetric zero-group velocity Lamb mode. This polarization is interpreted as the ratio of the absolute amplitudes of the surface normal and surface in-plane components of the mode. Results from the evaluation of simulated datasets indicate that the presented relation, which links the polarization and Poisson's ratio, can be extended to incorporate plates with material damping. Furthermore, the proposed application of the polarization is demonstrated in a practical field case, where an increased accuracy of estimated nominal thickness is obtained.

PACS numbers: 43.20.Ks, 43.40.Dx, 43.40.At.

1. Introduction

The fascinating properties of zero-group velocity (ZGV) Lamb modes [1, 2] have been demonstrated to be useful in several applications, such as measurements of acoustic bulk wave velocities and Poisson's ratio [3], thin-layer thickness [4], hollow cylinders [5], interfacial bond stiffness [6], and possibly air-coupled measurements [7]. In this study, we present a novel application of the amplitude ratio of the surface normal and the surface in-plane components, and demonstrate how it can be used to estimate Poisson's ratio. This investigation was carried out from the perspective of non-destructive testing of concrete structures under one-sided access test conditions, but our observations are also valid for any material and structure for which Lamb wave theory is a representative assumption.

The evaluation of the dynamic response to a transient impact is a common technique for estimation of the thickness and/or mechanical properties of plate-like concrete structures. This type of measurement technique, often referred to as an impact-echo measurement [8], employs the ZGV resonance frequency of the first symmetric (S1) Lamb mode [9]. To determine the thickness and/or mechanical properties, the frequency of the S1-ZGV mode must be complemented with two additional parameters, e.g. transverse wave speed and Poisson's ratio [10]. Combined impact-echo and surface wave measurements [11], where Poisson's ratio typically is determined from the longitudinal wave and the Rayleigh wave velocity [12], can be used to obtain these two additional parameters. However, systematic errors from near-field effects and velocity variation through the thickness can lead to an uncertain estimation of Poisson's ratio [11].

Alternative approaches that do not depend on an estimation of the longitudinal wave velocity are therefore important for accurate estimation of Poisson's ratio. One alternative strategy is to use the ratio between the S1-ZGV frequency and the minimum frequency of the second anti-symmetric Lamb mode [3]. This approach has been

demonstrated successfully for several thin homogenous metal plates [3], but only a few measurements have been reported for concrete plates [13].

To date, there is a lack of techniques that are independent of longitudinal wave velocity and that can accurately determine Poisson's ratio for concrete plates with only one accessible side. An interesting alternative is based on the polarization of Rayleigh waves [14]. Inspired by this idea of using polarization to estimate Poisson's ratio, here we propose and explore a new approach for estimating Poisson's ratio based on the polarization and shape of the S1-ZGV Lamb mode. An advantage of this new approach is that a through-thickness representative estimation of Poisson's ratio is obtained, since the S1-ZGV mode exists through the entire thickness of the plate.

This study is divided into three parts. We first present the theoretical foundation for this approach. We then verify the presented approach using a set of numerical simulations. Finally, we demonstrate the utility of this approach in a realistic field case.

2. Amplitude polarization of Lamb mode

According to Lamb wave theory, which defines linear elastic wave propagation along isotropic infinite plates, the possible combinations of angular frequencies ω and lateral wave numbers k that can exist in a free plate with a height h is defined by [10]:

$$\frac{\tan(\beta h/2)}{\tan(\alpha h/2)} = -\left[\frac{4\alpha\beta k^2}{(k^2-\beta^2)^2}\right]^{\pm 1} \tag{1}$$

where

$$\alpha^2 = \omega^2/V_L^2 - k^2$$
$$\beta^2 = \omega^2/V_T^2 - k^2$$

V_L and V_T are the longitudinal and transversal wave velocities, respectively. The positive sign of the exponent on the right side of Eq. (1) defines symmetric modes, whereas the negative sign defines anti-symmetric modes. The wave number k can be used to determine the displacement field of the plate. The amplitude for the displacement at the free surface for the surface in-plane U and surface normal W directions are given by [10]:

$$U = ck\left(\frac{1}{\tanh(qh/2)} - \frac{2qs}{k^2+s^2}\cdot\frac{1}{\tanh(sh/2)}\right) \tag{2}$$

$$W = -cq\left(1 - \frac{2k^2}{k^2+s^2}\right) \tag{3}$$

where c is an arbitrary multiplicative constant. The parameters q and s are calculated according to:

$$q = \sqrt{k^2 - k_L^2}\,, \quad s = \sqrt{k^2 - k_T^2}$$

where k_L and k_T are the longitudinal and transversal wave number, respectively.

Equation (1) was used to find the frequencies ω and wave numbers k of the S1-ZGV points corresponding to each value of Poisson's ratio ν in the range 0.1 to 0.4, with increments of 0.01. Variations in $|U|$ and $|W|$ as a function of ν are shown in Fig. 1(a). The arbitrary constant c, in this case the scaling of the curves, is selected to yield an amplitude of 1 for $|W|$ at $\nu = 0.1$. Fig. 1(b) displays the variation of the absolute ratio $|W/U|$ as a function of ν. This dimensionless quantity, which can be interpreted as the polarization of the S1-ZGV Lamb mode, is only dependent on ν, thus providing an opportunity to estimate ν if the polarization is measured. This relation is critical to the proposed approach.

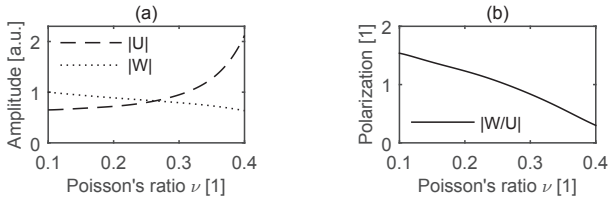

Fig. 1. (a) Absolute values of amplitudes components of S1-ZGV mode. (b) Polarization of S1-ZGV mode.

3. Numerical modeling

The relation in Fig. 1(b) is calculated without including material damping. However, in many practical applications such as measurements of concrete structures, material damping is present; from a theoretical point of view, true ZGV Lamb modes are in these cases strictly not defined [15]. For this reason, practical measurements were simulated to investigate whether the polarization relation in Fig. 1(b) can be used to estimate ν even though material damping is present. For simplicity, we hereafter use the S1-ZGV abbreviation to refer to the first thickness resonance of the plate, although, as mentioned previously, no true ZGV modes are strictly defined for absorbing plates.

An axially symmetric finite-element model was created with unit values for the thickness $h = 1\text{m}$, Young's modulus $E = 1\text{Pa}$, and density $\rho = 1\text{kg}/\text{m}^3$. Note that the analysis results of the simulations are independent of the exact values of h, E, ρ. Poisson's ratio was varied from 0.1 to 0.4, with increments of 0.01, and the loss factor η was varied from 0 to 0.05, with increments of 0.01. A short line load starting at the axial symmetric axis and with a length of $0.02h$ was applied at the top surface to simulate an applied point load. Since the S1-ZGV frequency is dependent on ν, the center frequency of the load (Gaussian mono pulse) was set equal to the theoretical S1-ZGV frequency for the corresponding plate without material damping. The model was solved in the frequency domain using a frequency-dependent mesh and absorbing region [16]. The time domain response was obtained from the inverse discrete Fourier transform of the frequency domain response.

Synthetic datasets were created for all combinations of varying ν and η. Figure 2(a) contains the dataset for $\nu = 0.1$ and $\eta = 0.01$. In this plot, the normalized time history (y axis) of the surface in-plane acceleration response is shown for various normalized radial offset locations r/h (x axis) at the top accessible surface. Each dataset consisted of 10 signals per length h within a radial distance of $4h$ from the axial symmetry axis. Similar to field measurements employing an impact point source, the broad frequency spectrum of the Gaussian mono pulse excites several Lamb modes. To reduce the influence from direct surface waves and enhance low group velocity modes (e.g. S1-ZGV), all signals were individually multiplied with a Tukey window. Figure 2(b) shows the amplitude of the window as function of time. The raw signals along with the windowed signals are shown in Fig. 2(a).

The mode shape at the S1-ZGV frequency was extracted using a temporal discrete Fourier transform of the windowed dataset. Figure 2(c) shows the absolute amplitude of the extracted mode at the S1-ZGV frequency for the surface in-plane and surface normal components as a function of the normalized radial distance r/h for the dataset with $\nu = 0.1$ and $\eta = 0.01$. Since the surface in-plane and surface normal components are not in phase, the polarization cannot be determined from two pointwise amplitudes at a fixed radial offset from Fig. 2(c) in a straightforward fashion. Instead, the spatial periodicity and amplitude for the total mode is used for simplicity

and robustness. For straight crested Lamb waves, the spatial periodicity is defined by the exponential function. However, in this case, Hankel functions are used to account for cylindrical spreading from a point source [17]. Accordingly, the analytical expressions for the absolute amplitude of the S1-ZGV mode shape as function of amplitudes U, W, wave number k, and radial distance r take the form:

$$A(U,k,r) = \left|\Re\left(|U|\,\mathrm{H}_1^{(1)}(kr)\,\mathrm{e}^{\mathrm{i}\arg(\mathrm{k})}\right)\right| \tag{4}$$

$$B(W,k,r) = \left|\Re\left(|W|\,\mathrm{H}_0^{(1)}(kr)\right)\right| \tag{5}$$

where A and B represent the surface in-plane and surface normal components, respectively. $H_1^{(1)}$ and $H_0^{(1)}$ are the first and zeroth-order Hankel functions of the first kind, respectively. We allow k to be complex-valued to account for material damping. The exponential term $\mathrm{e}^{\mathrm{i}\arg(\mathrm{k})}$ in Eq. 4 is introduced to maintain zero displacement at the axial symmetry axis ($r = 0$) when k is complex.

The absolute amplitudes $|U|$, $|W|$ and wave number k for the S1-ZGV mode of the simulated plate were estimated by searching for the best match between the analytic expressions in Eq. 4-5 and the extracted mode shape (markers in Fig. 2(c)). This search was carried out by minimizing the objective function:

$$f(U,W,k,r) = \sum_{i=1}^{N}\left(\frac{(a_i - A_i)^2}{|U|} + \frac{(b_i - B_i)^2}{|W|}\right) \tag{6}$$

where a_i and b_i are the absolute amplitudes of the surface in-plane and surface normal components of the extracted mode, respectively (markers in Fig. 2(c)). The index $i = 1, 2, ...N$ labels the simulated signals, where $i = 1$ represents the signal nearest the impact point. A_i and B_i represents the functions from Eq. 4-5 calculated at the radial offset $r = r_i$, i.e. $A_i = A(U,k,r = r_i)$ and $B_i = B(W,k,r = r_i)$. The function f was minimized by means of unconstrained nonlinear optimization using the *fminsearch* function available in MATLAB®. Good agreement was obtained between the best solution to the minimization problem and the extracted mode (Fig. 2(c)). The polarization was determined using $|W|$ and $|U|$ from this solution. This analysis, which enables the estimation of polarization, was repeated for each dataset (i.e. the simulated response to an impact pulse for the plate with varying combinations of ν and η). Figure 2(d) contains the estimated values of polarization for all datasets as well as the analytical relation (from Fig. 1(b)) calculated for lossless material. Good agreement exists between the analytical expression for the polarization and the simulated results. Note that the results from simulations that included material damping also match the analytical expression. Hence, the proposed approach is likely applicable to plates with material damping.

4. Field case

The proposed approach was tested on a concrete wall with a nominal thickness of 0.450 m. A three-component accelerometer attached to a fixed position on the wall was used to measure the response from hammer strokes performed at increasing offsets from the accelerometer. The input force from each stroke was also recorded. By using the reciprocity theorem for a linear elastic system, a multichannel dataset was obtained [11]. This dataset is of the same type as the simulated datasets in Section 3 and was processed in a similar way: a Tukey window was applied in the time domain, and then the absolute amplitude of the transfer function between the source and the receiver at the S1-ZGV frequency was extracted (Fig. 3(a)). The objective function f from Eq. 6 was minimized using the same technique as in Section 3. Figure 3(a) illustrates the matched functions A and B.

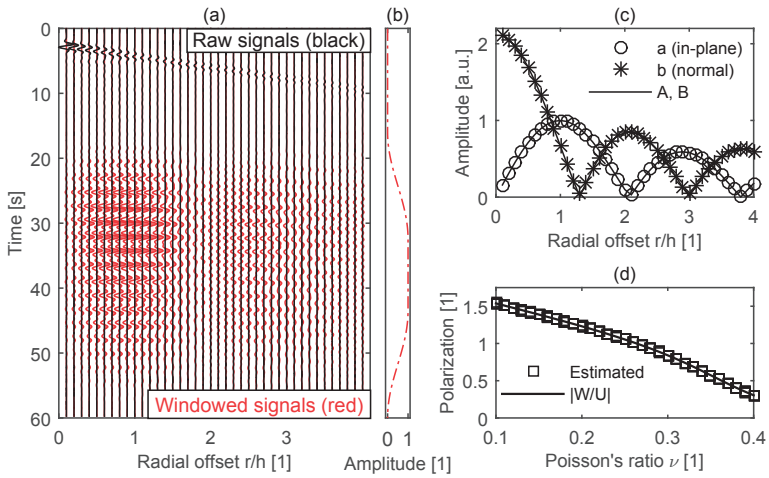

Fig. 2. (Color online) (a) Simulated multichannel dataset (surface in-plane component, $\nu = 0.1$, $\eta = 0.01$). (b) Tukey-window amplitude. (c) Absolute amplitude of extracted S1-ZGV mode (markers) and best solution (lines). (d) Estimated polarization (markers) and theoretical relation for lossless plates (solid line).

The polarization $|W/U|$ was estimated as 1.09, yielding $\nu = 0.24$. Unfortunately, no exact value of ν is accessible for comparison. However, the estimation of ν can be verified indirectly to a certain extent from the nominal thickness of the wall $h = 0.450\text{m}$. Estimation of the Rayleigh wave velocity (2430 m/s) from the raw signals displayed in frequency-phase velocity domain (Fig. 3(b)), the S1-ZGV frequency (4810 Hz) from the frequency spectrum of the windowed signal nearest the impact point (Fig. 3(c)), and Poisson's ratio (0.24) theoretically corresponds to a thickness of 0.447 m, which is within 1% error of the nominal thickness. The traditional approach [11] using the longitudinal wave velocity (4295 m/s) and Rayleigh wave velocity (2430 m/s), i.e. $\nu = 0.18$, theoretically corresponds to a thickness of 0.425, which is within 6% error of the nominal thickness. Thus, in this field case, our proposed approach provides a reasonable estimate of ν and an increased accuracy of the estimated nominal thickness, compared with the traditional approach.

5. Conclusions

Here we have presented a new approach to estimating Poisson's ratio from the amplitude polarization of the S1-ZGV Lamb mode. Numerical simulations demonstrated that this approach is also applicable to plates with material damping. A field-case example illustrated a benefit of this approach: a through-thickness representative value for Poisson's ratio is obtained via this strategy, thereby improving the overall estimation of plate parameters under one-sided access test conditions.

Acknowledgments

The Development Fund of the Swedish Construction Industry (SBUF, No. 12534) and The Swedish Radiation Safety Authority (SSM, No. SSM2012-890) are acknowledged for financing the study.

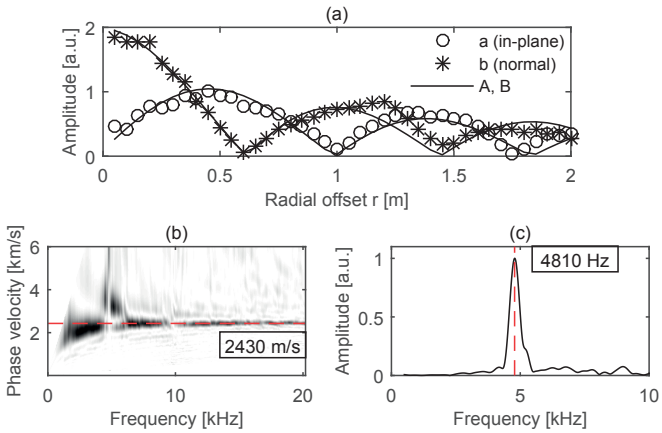

Fig. 3. (Color online) (a) Absolute amplitude of extracted S1-ZGV mode (markers) and best solution (lines). (b) Frequency-phase velocity spectrum, and estimated Rayleigh wave velocity (dashed line). (c) Frequency spectrum of (windowed) surface normal component signal nearest impact point (solid line), and estimated S1-ZGV frequency (dashed line).

References and links

[1] Eduardo Kausel. Number and location of zero-group-velocity modes. *The Journal of the Acoustical Society of America*, 131(5):3601–10, May 2012. ISSN 1520-8524. doi: 10.1121/1.3695398.

[2] Claire Prada, Dominique Clorennec, and Daniel Royer. Local vibration of an elastic plate and zero-group velocity Lamb modes. *The Journal of the Acoustical Society of America*, 124(1):203–12, July 2008. ISSN 1520-8524. doi: 10.1121/1.2918543.

[3] Dominique Clorennec, Claire Prada, and Daniel Royer. Local and noncontact measurements of bulk acoustic wave velocities in thin isotropic plates and shells using zero group velocity Lamb modes. *Journal of Applied Physics*, 101(3):034908, 2007. ISSN 00218979. doi: 10.1063/1.2434824.

[4] Maximin Cès, Dominique Clorennec, Daniel Royer, and Claire Prada. Thin layer thickness measurements by zero group velocity Lamb mode resonances. *The Review of scientific instruments*, 82(11): 114902, November 2011. ISSN 1089-7623. doi: 10.1063/1.3660182.

[5] M Cès, D Royer, and C Prada. Characterization of mechanical properties of a hollow cylinder with zero group velocity Lamb modes. *The Journal of the Acoustical Society of America*, 132(1):180–5, July 2012. ISSN 1520-8524. doi: 10.1121/1.4726033.

[6] Chia-Chi Cheng, Chih-Peng Yu, and Tzunghao Liou. Evaluation of interfacial bond condition between concrete plate-like structure and substrate using the simulated transfer function derived by IE. *NDT & E International*, 42(8):678–689, December 2009. ISSN 09638695. doi: 10.1016/j.ndteint.2009.06.001.

[7] Stephen D. Holland and D. E. Chimenti. Air-coupled acoustic imaging with zero-group-velocity Lamb modes. *Applied Physics Letters*, 83(13):2704, 2003. ISSN 00036951. doi: 10.1063/1.1613046.

[8] M.J. Sansalone and W.B. Streett. *Impact-echo: Non-destructive Evaluation of Concrete and Masonry*. Bullbrier Press, 1997.

[9] Alexander Gibson and JS Popovics. Lamb wave basis for impact-echo method analysis. *Journal of Engineering mechanics*, pages 1–6, 2005. doi: 10.1061/(ASCE)0733-9399(2005)131:4(438).

[10] Igor Aleksandrovich Viktorov. *Rayleigh and Lamb Waves Physical Theory and Applications*. Plenum Press, New York, 1967.

[11] Oskar Baggens and Nils Ryden. Systematic errors in Impact-Echo thickness estimation due to near field effects. *NDT & E International*, 69:16–27, January 2015. ISSN 09638695. doi: 10.1016/j.ndteint.2014.09.003.

[12] TT Wu, JS Fang, GY Liu, and MK Kuo. Determination of elastic constants of a concrete specimen using transient elastic waves. *The Journal of the Acoustical Society of America*, 98(4):2142–2148, 1995.

[13] Alexander Gibson. *Advances in Nondestructive Testing of Concrete Pavements*. Ph.d. thesis, University of Illinois, 2004.

[14] Ana Bayon, Francisco Gascon, and Francisco J. Nieves. Estimation of dynamic elastic constants from the amplitude and velocity of Rayleigh waves. *The Journal of the Acoustical Society of America*, 117 (6):3469, 2005. ISSN 00014966. doi: 10.1121/1.1898663.

[15] F. Simonetti and M. J. S. Lowe. On the meaning of Lamb mode nonpropagating branches. *The Journal of the Acoustical Society of America*, 118(1):186, 2005. ISSN 00014966. doi: 10.1121/1.1938528.

[16] M. Castaings, C. Bacon, B. Hosten, and M. V. Predoi. Finite element predictions for the dynamic response of thermo-viscoelastic material structures. *The Journal of the Acoustical Society of America*, 115(3):1125, 2004. ISSN 00014966. doi: 10.1121/1.1639332.

[17] JJ Ditri and A Pilarski. Generation of guided waves in a plate by axisymmetric normal surface loading. *Review of Progress in Quantitative Nondestructive Evaluation*, 13, 1994.

Printed by Media-Tryck, Lund University 2015

Lund University
Division of Engineering Geology

ISBN 978-91-7623-259-0 (print)
ISBN: 978-91-7623-260-6 (web/pdf)
ISRN LUTVDG/TVTG-1033)/1-93/2015